Biophysical Journal
Article

Biophysical Society

High rates of calcium-free diffusion in the cytosol of living cells

Cecilia Villarruel,[1,2,3] Pablo S. Aguilar,[1,2] and Silvina Ponce Dawson[3,*]
[1]Laboratorio de Biología Celular de Membranas, Instituto de Investigaciones Biotecnológicas, Universidad Nacional de San Martín, San Martín, Argentina; [2]Instituto de Fisiología, Biología Molecular y Neurociencias, Universidad de Buenos Aires (UBA) and [3]Departamento de Física, Facultad de Ciencias Exactas y Naturales, UBA, and Instituto de Física de Buenos Aires, CONICET, Ciudad Auntónoma de Buenos Aires, Argentina

ABSTRACT Calcium (Ca^{2+}) is a universal second messenger that participates in the regulation of innumerous physiological processes. The way in which local elevations of the cytosolic Ca^{2+} concentration spread in space and time is key for the versatility of the signals. Ca^{2+} diffusion in the cytosol is hindered by its interaction with proteins that act as buffers. Depending on the concentrations and the kinetics of the interactions, there is a large range of values at which Ca^{2+} diffusion can proceed. Having reliable estimates of this range, particularly of its highest end, which corresponds to the ions free diffusion, is key to understand how the signals propagate. In this work, we present the first experimental results with which the Ca^{2+}-free diffusion coefficient is directly quantified in the cytosol of living cells. By means of fluorescence correlation spectroscopy experiments performed in *Xenopus laevis* oocytes and in cells of *Saccharomyces cerevisiae*, we show that the ions can freely diffuse in the cytosol at a higher rate than previously thought.

SIGNIFICANCE Intracellular calcium signals are ubiquitous. Their versatility depends on the way in which local elevations of the cytosolic calcium concentration spread in space and time. The calcium diffusion coefficient is key in this regard. Calcium diffusion in the cytosol is hindered by the binding and unbinding of the ions with less mobile species. If the calcium concentration is high enough, calcium diffusion proceeds at its free rate. Having reliable estimates of the range of diffusion rates in situ is unavoidable for any quantitative modeling of calcium signals. In this work, we quantify directly the free diffusion coefficient of calcium in intact *Xenopus laevis* oocytes and in budding yeast live cells, finding that the ions can diffuse faster than previously thought.

INTRODUCTION

Calcium (Ca^{2+}) is a ubiquitous intracellular messenger involved in the regulation of diverse biological processes (1). The versatility of Ca^{2+} signals relies on the variety of spatiotemporal distributions of the cytosolic [Ca^{2+}] that elicit different end responses (2–5). Prolonged high elevations of cytosolic [Ca^{2+}] can lead to cell death (1,6). For this reason, cells have various mechanisms to keep its basal concentration at a very low (~20–200 nM) level. Specialized proteins pump Ca^{2+} into internal stores, whereas others extrude it into the extracellular milieu. In vertebrates, the endoplasmic reticulum (ER) and sarcoplasmic reticulum are the principal Ca^{2+} internal stores, although mitochondria also take up Ca^{2+} (6). In budding yeast, the principal Ca^{2+} reservoir is the vacuole; the Golgi Apparatus and the ER are involved in the maintenance of Ca^{2+} basal levels by means of Ca^{2+} pumps and antiporter proteins that also provide Ca^{2+} to these organelles (7,8). The fastest way in which cells decrease their cytosolic [Ca^{2+}] is by means of Ca^{2+} buffers (9), typically proteins, that bind Ca^{2+}, modifying its free concentration and its transport rate (10–12). Intracellular Ca^{2+} signals are thus the result of the interplay of Ca^{2+} entry through specialized channels located either on the plasma membrane or the membrane of internal stores and the various processes that tend to reduce the cytosolic [Ca^{2+}] and Ca^{2+} diffusion. Given a point of entry, the spatial range of the [Ca^{2+}] elevation, which is delimited by the ions transport rate, then determines the eventual end response. Because of the reactions with the various buffers, the ions transport rate in the cytosol is not solely

Submitted February 10, 2021, and accepted for publication August 11, 2021.

*Correspondence: silvina@df.uba.ar

Editor: Alberto Diaspro.
https://doi.org/10.1016/j.bpj.2021.08.019

due to their free diffusion, the process that arises when (dilute) solute particles randomly change their direction of movement upon collision with solvent molecules (13,14). Under certain conditions, the net transport can be described in terms of effective diffusion coefficients that depend on the reaction rates with the buffers and on the concentrations and free diffusion coefficients of the interacting species (15–17). In the case of Ca^{2+}, these effective rates go from very low values at basal conditions to values closer to the ions free diffusion rate upon buffer saturation. Thus, the effective coefficients change with [Ca^{2+}] and, during the time course of a Ca^{2+} signal, are space and time dependent. It is the upper limit of the range of possible values, the free diffusion coefficient, that should remain fairly constant under various conditions. Knowing the range of possible values is relevant, especially for the understanding of situations in which the spatiotemporal distribution of intracellular Ca^{2+} is a key aspect of the signaling, as in frequency-encoded responses (18), long distance coupling phenomena (19,20), or at the transition to propagating either intra- (21–24) or inter- (25,26) cellular Ca^{2+} waves. The direct quantification of the Ca^{2+} diffusion coefficient and of how it varies through the interaction with buffers in living cells is therefore of utmost importance.

The rate at which Ca^{2+} diffuses in the cytosol was estimated in Allbritton et al. (16) using cytosolic extracts of *Xenopus laevis* oocytes and radioactive Ca^{2+}, $^{45}Ca^{2+}$. The experiments of Allbritton et al. (16) were done by adding $^{45}Ca^{2+}$ at one end of a test tube containing the cytosolic extract (previously equilibrated with different nonradioactive [Ca^{2+}]) and then measuring the spatial spread of the radioactivity with time. The diffusion coefficient derived for the largest values of nonradioactive [Ca^{2+}] probed in Allbritton et al. (16), 220 $\mu m^2/s$, has been considered an estimate of the Ca^{2+}-free diffusion coefficient, D_{Ca}, in cells and has been widely used in mathematical models of intracellular Ca^{2+} dynamics. One important caveat in Allbritton et al. (16) analyses is that $^{45}Ca^{2+}$ ions interactions with buffers displace pre-existing nonradioactive ions, which in turn, also contribute to signal propagation but are experimentally invisible. In this sense, it has been shown that the effective rates with which $^{45}Ca^{2+}$ diffuses in experiments like those in Allbritton et al. (16) are lower than those that would have been calculated measuring both contributing ions, radioactive and nonradioactive Ca^{2+} (17). Considering these analyses, it is legitimate to ask whether the largest value obtained by Allbritton et al. (16) underestimates the Ca^{2+}-free diffusion coefficient. In Allbritton et al. (16), this estimate was compared with the (free) diffusion coefficient of inositol 1,4,5-trisphosphate (IP_3), a co-agonist (with Ca^{2+}) of IP_3 receptors (IP_3R) (27–29), a type of Ca^{2+} channel that is located on the membrane of the vertebrate cells ER. Because of regulation of cytosolic Ca^{2+}, IP_3R-mediated signals are subject to calcium-induced calcium release (30), by which the Ca^{2+} released through one open IP_3R induces the opening of nearby ones. Because high cytosolic Ca^{2+} also inhibits IP_3Rs, whether IP_3 or Ca^{2+} reaches the IP_3Rs first can thus determine whether a Ca^{2+} wave can propagate or not. In Allbritton et al. (16), the free IP_3 diffusion coefficient was estimated as ~280 $\mu m^2/s$, i.e., larger than D_{Ca}. More recent experiments (31) have shown that IP_3 diffusion in the cytosol is also hindered by trapping mechanisms; values similar to the effective diffusion rate of buffered Ca^{2+} (~5 $\mu m^2/s$) were estimated in Dickinson et al. (31). In view of these results, the question of what is the range within which the transport rates of Ca^{2+} and IP_3 can vary in living cells becomes most relevant. Having a reliable estimate of D_{Ca} in the cytosol is also relevant outside the context of IP_3R-mediated Ca^{2+} signals. In particular, we think it is key to understand the Ca^{2+}-dependent responses in *Saccharomyces cerevisiae* to external cues (32–35), especially for the recently observed Ca^{2+} pulses that are elicited in response to the presence of the sexual pheromone (18).

Another limitation of the experiments of Allbritton et al. (16) is that they were performed in cytosolic extracts. Ca^{2+} diffusion in live cells was analyzed with experiments in which caged Ca^{2+} was photo-released and subsequently observed using a Ca^{2+} indicator (36). These observations, however, correspond to the fluorescence emitted by the Ca^{2+}-bound dye. Going from the observed signal to the underlying Ca^{2+} spatiotemporal distribution is not completely straightforward; it requires a detailed model (37) and having reliable estimates of various biophysical parameters that are frequently unknown (38–40). To address these limitations for this work, we performed fluorescence correlation spectroscopy (FCS) experiments with which we estimate the Ca^{2+}-free diffusion coefficient in intact cells without the need of any previous knowledge of other biophysical parameters.

FCS is an optical technique that uses the statistical analysis of fluorescence fluctuations in a small detection volume to quantify the processes that underlie the fluctuations (41). In combination with confocal microscopy, FCS has been widely used to estimate diffusion coefficients, concentrations, and reaction rates (42–44). These estimates are derived from the correlation times that characterize the autocorrelation function (ACF) of the fluorescence fluctuations. The direct application of this technique to the case of Ca^{2+} transport in live cells is not completely straightforward; intracellular Ca^{2+} is observed indirectly monitoring sensors that change their fluorescence properties upon Ca^{2+} binding (45,46) and that compete with the intracellular Ca^{2+} buffers disrupting the normal time course of the underlying processes (12,47). Our previous work on FCS experiments using a single-wavelength (SW) Ca^{2+} sensor to monitor Ca^{2+} in aqueous solutions (48) and in solutions containing the Ca^{2+} chelator, EGTA, as well (49) showed that it was possible to derive the free diffusion coefficients of the nonfluorescent species (Ca^{2+} and EGTA) from the correlation times. The

theoretical studies of Villarruel and Dawson (50) explained why this was possible. In this work, we build upon these previous works and present the results of FCS experiments performed in *X. laevis* oocytes and in live *S. cerevisiae* cells using chemical and genetically encoded fluorescent Ca^{2+} sensors, respectively. In this way, quantifying directly the Ca^{2+}-free diffusion coefficient, we have found that the Ca^{2+} ions can freely diffuse in the cytosol at a faster rate than previously thought.

MATERIALS AND METHODS

Cells

S. cerevisiae

SFmCherry-GCaMP6f expression vector construction. A vector expressing a dual sensor composed by the Ca^{2+} sensor green fluorescent protein-calmodulin fusion protein 6f (GCaMP6f) fused to the superfolder monomeric Cherry (SFmCherry) was constructed. The yeast integrative vector pRS306K-GPD1p-GCaMP6f-ADH1t-a (18) was used as template to perform restriction free cloning reactions (51) designed to insert SFmCherry and a short and flexible linker open reading frame in GPD1p-GCaMP6f. Then, a longer and rigid linker based on the aminoacid sequence of ER/K ((52,53) plasmids and oligos sequences available upon request) was inserted by RF cloning reactions in SFmCherry-GCaMP6f in the middle of the short linker to avoid Förster resonance energy transfer between the two proteins (54) (see Fig. S1). The final vector was verified by sequencing and subsequently linearized for yeast transformation.

Yeast strain and growth conditions. The strains used in this work are in the W303 background (leu2-3, 112 trp1-1 can1-100 ura3-1 ade2-1 his3-11). Cells were grown at 30°C in either rich yeast extract-Peptone-Dextrose (YPD) medium (1% yeast extract, 2% Bacto-peptone, and 2% glucose) or synthetic defined medium containing 0.67% yeast nitrogen base without amino acids (Difco Laboratories, Franklin Lakes, NJ), 2% glucose, and the appropriate drop-out mixture (mix) of amino acids, according to supplier's instructions (Complete Supplemental Mixture; Sunrise Science Products, Knoxville, TN). In general, yeast strains were grown in 3 mL of rich medium YPD to an optical density at 600 nm (OD600) of 0.2–0.6 and then were cultured for a minimum of 18 h in synthetic defined medium and supplemented with 80 ng/mL adenine and tryptophan (Sigma-Aldrich, St. Louis, MO) at 30°C to OD600 = 0.3–0.5. For imaging, 200 μL of cell culture was incubated in concanavalin-A (Sigma-Aldrich)-coated chambers for 10 min (number 1.5 glass; MatTek, Ashland, MA). Finally, synthetic defined medium was replaced by a fresh one, and cells were imaged. To generate a rise of cytoplasmic Ca^{2+}, 20 μL of $CaCl_2$ 2 M were added to the medium (final volume, 220 μL) (55). Data were acquired during the first 5 min after the $CaCl_2$ addition so as to prevent the mounting of the cell's response to the increase in Ca^{2+} (55). Membrane integrity was previously verified in all cases.

X. laevis oocytes

X. laevis oocytes, previously treated with collagenase and stored in Barth's solution (88 mM NaCl, 1 mM KCl, 2.4 mM $NaHCO_3$, 0.82 mM $MgSO_4$, 0.33 mM $Ca(NO_3)_2$, 0.14 mM $CaCl_2$, 5 mM HEPES, 0.05 mg/mL gentamycin (pH 7.4)) at 18°C, were loaded with 37 nL of a solution containing the Ca^{2+} indicator Fluo8 (Abcam, Cambridge, UK) and, for some experiments, the Ca^{2+} chelator EGTA. Fluo8 is a SW green fluorescent Ca^{2+} indicator, with a molecular weight of 877 g/mol and k_D = 432 and 600 nM in vitro and in vivo, respectively. It has a >100 times fluorescence enhancement when bound to Ca^{2+}. Its excitation maximum is at 488 nm, and its emission maximum is at 525 nm. EGTA has dissociation constant kD = 140 nM and diffusion coefficient in solution D = 405 $\mu m^2/s$. The concentration of Fluo8 in the microinjected solution was 100 μM or 1 mM, and the concentration of EGTA was between 1.25 and 10 mM. Assuming a 1 μL cytosolic volume, the final concentration of Fluo8 was 3.7 and 37 μM, respectively, and that of EGTA ranged within 47–370 μM. Injections were performed at the equator of the cell. Microinjections were done using a Drummond Nanoject II microinjector (Drummond Scientific, Broomall, PA) with an injection speed of 26 nL per second. Solutions to be injected were backfilled into glass micropipettes obtained by heat stretching of Borosilicate Drummond capillaries (7″ long, 0.53 mm internal diameter, and 1.14 mm external diameter) with a Puller PC-10 (Narishigue, Amityville, NY), which uses a heat method and vertical stretching by force of gravity. Oocytes were mounted on an aluminum chamber with a coverslip at the bottom for microscopic observations. Oocytes were deposited with the animal hemisphere down and immersed in Barth's solution. To avoid photodamage of the ER membrane and the consequent Ca^{2+}liberation, FCS measurements were performed at 3 μm from the granules zone.

Data acquisition

Fluorescence records were obtained at room temperature (~20°C) in a spectral confocal scanning microscope FluoView 1000 (Olympus, Tokyo, Japan) with a photomultiplier detector, using a 60× oil immersion objective (UPlanSApo), NA 1.35, and a 115 μm pinhole size.

S. cerevisiae cells

The sample was illuminated with the 488 nm line of an Argon laser with an excitation power of 6–10 μW and the 543 nm line of a Helium-Neon laser with an excitation power of 2 μW. Cells were not simultaneously illuminated with the two laser lines because the SFmCherry protein gets bleached with the 488 nm laser line. The fluorescence was collected from a single point located at ~2 μm from the coverslip at a 100/50 kHz acquisition rate during ~10.8/21.6 s (equivalently, 1,024,000 data points) in the 500–530/580–630 nm range for the 488/543 nm lines (green/red channel).

X. laevis oocytes

The sample was illuminated with the 488 nm line of an Argon laser with an excitation power of 6–10 μW. The fluorescence was collected from a single point located at ~15 μm from the coverslip at a 50 kHz acquisition rate during ~180 s (equivalently, 8,388,096 data points) in the 500–600 nm range.

Calibration of the observation volume

The confocal volume was calibrated for each configuration. 100 nM of fluorescein (Sigma, St. Louis, MO) in a buffer solution (pH 9) was used to determine the lateral widths of the effective volume at 15 and 2 μm from the coverslip for the 488 nm line. 100 nM of 10 kDa tetramethylrhodamine dextran (TMR-D; Sigma-Aldrich) in a buffer solution (pH 9) was used to determine the widths at 2 μm from the coverslip for the 543 nm line. The calibrations were done assuming that the diffusion coefficients of fluorescein and TMR-D were 425 (56) and 85 $\mu m^2/s$ (57), respectively. The resulting values of the lateral widths were w_r = (0.311 ± 0.002) μm and w_r = (0.1581 ± 0.0047) μm for the 488 nm line at 15 and 2 μm from the coverslip, respectively, and w_r = (0.1623 ± 0.0048) μm for the 543 nm line. The widths derived from the calibration at 15 μm from the coverslip were used in the experiments performed in oocytes, and those obtained at a 2-μm distance for the 488 nm and 543 nm lines were used in the experiments performed in yeast observed in the green and red channels (Gch and Rch), respectively.

Data analysis

Computation of the ACF

The ACF of the fluorescence fluctuations, $G(\tau)$, is given by:

$$G(\tau) = \frac{\langle \delta f(t) \delta f(t+\tau) \rangle}{\langle f(t) \rangle^2}, \quad (1)$$

where $f(t)$ is the fluorescence collected from the observation volume at time t, $\langle f(t) \rangle$ is its mean value, and $\delta f(t)$ is the deviation with respect to this mean at each time, t. To compute the experimental ACF N-long fluorescence record ($N = 8{,}388{,}096$ for oocytes and $N = 1{,}024{,}000$ for yeast), fluorescence record was divided into segments of $N_l = 2^{13}$ time points each. An ACF was computed for each of these N/N_l segments as:

$$G_k(\tau) = \sum_{i=1+(k-1)N_\ell}^{kN_\ell} \frac{\left(f(t_i) - \overline{f}_k\right)\left(f(t_i+\tau) - \overline{f}_k\right)}{\overline{f}_k^2},$$

$$\overline{f}_k = \sum_{i=1+(k-1)N_\ell}^{kN_\ell} f(t_i), \quad 1 \le k \le N/N_\ell, \quad (2)$$

adding zeros as needed, and then the average over the G_ks was performed. This was done using custom-made routines on Matlab (The MathWorks, Natick, MA) (58). The average ACFs were fitted with different expressions as explained in what follows using the *nlinfit* function of Matlab (58). To avoid the effects of after-pulsing, the first one to three points of the experimental ACF were not considered for the fitting.

Fitting the ACF

To fit the ACFs obtained with fluorescein, TMR-D, or SFmCherry, we used the analytic expression that corresponds to a freely diffusive fluorophore that does not change its fluorescence properties with binding (see e.g., (59)):

$$G_{fit,1}(\tau) = \frac{A_1}{\left(1 + \frac{\tau}{\tau_1}\right)\sqrt{1 + \frac{\tau}{w^2\tau_1}}}, \quad (3)$$

i.e., a one-component model, where $w = w_z/w_r$ is the aspect ratio of the sampling volume, and w_z and w_r are the sizes of the beam waist along z and r, with z the spatial coordinate along the beam propagation direction and r a radial coordinate in the perpendicular plane. τ_1 is the correlation time, which is related to the diffusion coefficient of the sample.

To fit the ACFs obtained with Fluo8 and GCaMP6f, we tried different forms, with two or three components, that had been used to analyze FCS data obtained from experiments in aqueous solutions with Ca^{2+} and a SW Ca^{2+} indicator (48,49):

$$G_{fit,2}(\tau) = \frac{A_1}{\left(1 + \frac{\tau}{\tau_1}\right)\sqrt{1 + \frac{\tau}{w^2\tau_1}}} + \frac{A_2 e^{-\nu_2 \tau}}{\left(1 + \frac{\tau}{\tau_2}\right)\sqrt{1 + \frac{\tau}{w^2\tau_2}}}. \quad (4)$$

$$G_{fit,3}(\tau) = \frac{A_1}{\left(1 + \frac{\tau}{\tau_1}\right)\sqrt{1 + \frac{\tau}{w^2\tau_1}}} + \frac{A_2 e^{-\nu_2 \tau}}{\left(1 + \frac{\tau}{\tau_2}\right)\sqrt{1 + \frac{\tau}{w^2\tau_2}}} + \frac{A_3 e^{-\nu_3 \tau}}{\left(1 + \frac{\tau}{\tau_3}\right)\sqrt{1 + \frac{\tau}{w^2\tau_3}}}. \quad (5)$$

In particular, when the ACFs derived from the experiments performed in aqueous solutions with Fluo8 and Ca^{2+} and in oocytes at basal conditions (i.e., with no EGTA added) and the ACFs obtained for the fluorescence detected in the Gch in the case of yeast (emission from GCaMP6f) were fitted with a three-component model (Eq. 4), the diffusion coefficient derived from τ_1 and τ_1 were indistinguishable. That is why in such cases, we present the results obtained by fitting the ACFs with a two-component model (Eq. 4). For the ACFs obtained from experiments performed in oocytes injected with Fluo8 and EGTA, we present the fits obtained with a three-component model (Eq. 5).

In all cases, we used $w = w_z/w_r = 5$, and the width, w_r, is derived from a calibration as explained before.

The goodness of the fit was evaluated computing the difference between the experimental ACFs, $G(\tau)$, and the fits, $G_{fit}(\tau)$, as:

$$\chi^2 = \frac{1}{N_\ell} \sum_{i=1}^{N_\ell} \frac{\left(G_{fit}((i-1)d\tau) - G((i-1)d\tau)\right)^2}{G_{fit}((i-1)d\tau)}, \quad (6)$$

where $d\tau$ is the fluorescence acquisition time, and N_l is the total number of data points of the experimental ACF.

Analysis of the fitted parameters

The diffusion coefficients, D_i, were derived from the fitted correlation times, τ_i, as:

$$\tau_i = \frac{w_r^2}{4D_i}. \quad (7)$$

As explained in the Supporting materials and methods, in reaction-diffusion systems, these are actually effective diffusion coefficients, although they can be well approximated by free diffusion ones depending on the conditions.

The estimates derived for a given parameter could be different depending on the analyzed record. To study this variability, we generated histograms of the fitted parameters, binning the data in 10 equally spaced intervals. On some occasions, the histograms looked as if there was more than one population of parameters. To analyze this aspect, we applied the Akaike criterion (60) to determine if the underlying parameter distribution was uni or bimodal, employing the *gmdistribution.fit* function of Matlab. This function was used to estimate the parameters of a model distribution with one or two Gaussian components and to obtain the Akaike information criterion of each of these models. We then calculated the Akaike criterion's difference (Ak_D) between both models. The values of Ak_D range from -1 to 1, with positive values suggesting bimodality and negative values suggesting unimodality. Results from the fittings are reported as mean ± SE for unimodal distributions and as mean and fraction of the total distribution (between parentheses) and Ak_D for bimodal ones. The subscripts a and b were used to identify the mean diffusion coefficient of each population. To decide whether the data followed a uni or bimodal distribution, not only the Ak_D was taken into account but also the proportion and the data distribution inside each group.

Numerical computations

We calculated the expected (theoretical) effective diffusion coefficients for reaction-diffusion systems with Fluo8 and Ca^{2+} and with Fluo8, EGTA, and Ca^{2+} as done in Sigaut et al. (48,49) using the parameters of Table 1 (also see Supporting materials and methods) and the following concentrations: $[\text{Fluo8}]_{tot}$ = 3.7 or 37 μM, $[\text{EGTA}]_{tot}$ = (0–370) μM, and $[Ca^{2+}]_{eq}$ = 100 nM. The notation $[X]_{tot}$ indicates the total concentration of species, X, i.e., the sum of its free and all of its bound forms. The notation $[Ca^{2+}]_{eq}$ refers to the free Ca^{2+} concentration in equilibrium with the other species of the system with which it interacts. The various diffusion coefficients listed in the tables (D_X) are free diffusion coefficients of the corresponding species, X, in aqueous solutions. We assume that the ratio between any two

TABLE 1 Parameters used for the computations corresponding to a system with Fluo8 and Ca^{2+} or Fluo8, EGTA, and Ca^{2+}

Parameter	Value
D_{Fluo8}	100 $\mu m^2/s$
D_{EGTA}	405 $\mu m^2/s$
D_{Ca}	760 $\mu m^2/s$ (61)
kD_{Fluo8}	432[a] and 600[b] nM
$koff_{Fluo8}$	45[a] and 70[b] s^{-1}
kD_{EGTA}	150 nM
$koff_{EGTA}$	0.75 s^{-1}

The diffusion coefficients correspond to free diffusion of each species in aqueous solution.
[a]The reaction constants correspond to aqueous solution.
[b]The reaction constants correspond to situations in vivo. In the case of the reaction EGTA-Ca^{2+}, we do not make this distinction.

of these free coefficients remains the same in aqueous solution and in the cytosol. It is implicit in this assumption that the free coefficients change with viscosity (and temperature) in such a way that their ratios do not. We assume that the reaction between Ca^{2+} and any of the other species, X, is of the form:

$$Ca + X \underset{kon_X}{\overset{koff_X}{\rightleftarrows}} CaX, \tag{8}$$

with dissociation constant $kD_X = koff_X/kon_X$. The off-rate and the dissociation constants are listed in Table 1. For the computation of the effective coefficients, we assumed that the free diffusion coefficient of each species, X, that interacts with Ca^{2+} is the same in its free and its Ca^{2+}-bound form (i.e., $D_X = D_{CaX}$). In the case of the computations in the cytosol, we either rescaled all the diffusion coefficients by a common factor or divided all by the largest one obtained at each condition probed. For the first type of rescaling, we estimated the Ca^{2+}-free diffusion coefficient in the cytosol from the experiments and calculated the rescaling factor as the ratio between this estimate and the value, D_{Ca}, of Table 1. In the second case, we compared the theoretical ratios with similar ones between the average coefficients derived from the experiments at each condition probed. Proceeding in this way is meaningful under the assumption that the ratios between the free diffusion coefficients are the same in solution and in the cytosol. These computations allowed us to relate the coefficients derived from the experimental fits with those that are acting in the system under study.

RESULTS

The design of the experiments described in this section was inspired by our previous work (48–50) on the use of FCS in aqueous solutions in which the fluorescence was emitted by SW Ca^{2+} sensor. These sensors increase their fluorescence intensity by a large factor when bound to Ca^{2+} (45). In these experimental setups, the fluorescence fluctuations not only depend on the transport of the sensor in and out of the observation volume but also on its binding reaction with Ca^{2+}. Our previous work showed that the characteristic times of some of the processes that shape the free [Ca^{2+}], such as diffusion and binding-unbinding reactions, are reflected on the correlation times of the fluorescence fluctuations ACF. The best fits of the experimental ACFs of Sigaut et al. (48,49) and Villarruel and Dawson (50) were characterized by two diffusive timescales that we could associate either to free or effective diffusion coefficients of the problem. Varying the concentration of one of the reactants, we determined if the derived coefficients were free (if they remained constant) or effective (if they changed). We describe in what follows how we proceeded with the two used cell types and the results that we obtained.

FCS experiments in *S. cerevisiae* cells

In this work, we used a modified version of the Ca^{2+} sensor GCaMP6f, which was originally developed to monitor neuronal activity and which we have already adapted to *S. cerevisiae* (18). To count with a Ca^{2+} sensor that was better suited to our FCS experiments, we fused GCaMP6f to SFmCherry, which is Ca^{2+} insensitive. Provided that there is no energy transfer between the two linked fluorophores (see Fig. S1), the fluctuations of the fluorescence coming from the latter should only depend on the transport properties of the sensor in and out of the observation volume, i.e., they serve to determine its free diffusion coefficient.

First, we performed FCS experiments in SFmCherry-LL-GCaMP6f expressing *S. cerevisiae* cells when the fluorescence was excited with the 543 nm line and collected in the Rch (580 − 630 nm). This emission comes from the SFmCherry part of the sensor. Because we expect the diffusion coefficient of SFmCherry-LL-GCaMP6f to be unaltered upon Ca^{2+} binding (given the small fraction of the protein mass that an individual ion represents), we assumed that the corresponding SFmCherry ACF is solely characterized by one correlation time: the one associated to the free diffusion coefficient of the sensor. For this reason, this set of experimental results was fitted using a one-component model expressed in Eq. 3. We show in Fig. 1 *A* the example of an ACF obtained in this case and the corresponding fit. From the fits over 248 ACFs, we derived the SFmCherry-LL-GCaMP6f diffusion coefficient, $D_1 = (8 \pm 0.25)\ \mu m^2/s$. The histogram (in frequency) of the derived D showed a relatively long tail toward the largest values (Fig. 1 *B*). The application of the Akaike criterion (see Materials and methods) gave a positive value for the Ak_D ($Ak_D = 0.0613$). The obtained means of the two subpopulations were $D_{1a} = 7\ \mu m^2/s$ and $D_{1b} = 12\ \mu m^2/s$, with proportions, 70 and 30%, respectively. As discussed later, the difference can be attributed to heterogeneous cytoplasmic viscosity (62–66). These values are compatible with the ones previously estimated for cytosolic proteins in living yeast cells (67) and with those derived from the observations in the Gch (see below), indicating that we were able to infer the free diffusion coefficient of this genetically encoded Ca^{2+} sensor.

Subsequently, we performed FCS experiments as previously but illuminating the cells with the 488 nm line of an Argon laser and observing the fluorescence coming from the GCaMP6f part of the sensor in the 500–530 nm range. We show in Fig. 2 *A* an example of the ACF obtained in this way when the cells were incubated in synthetic complete

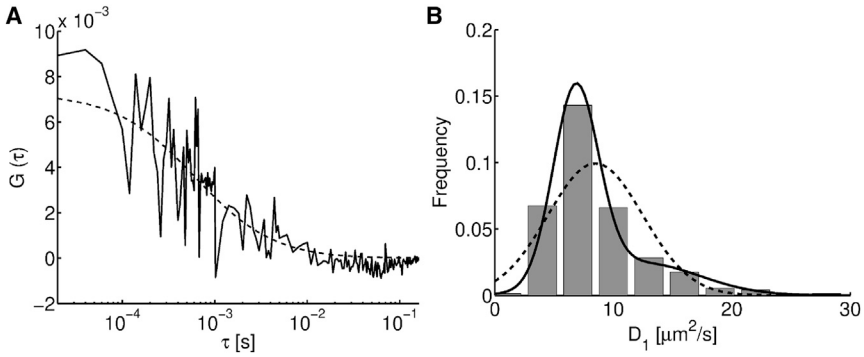

FIGURE 1 FCS experiments to estimate the free diffusion coefficient of the Ca^{2+} dual sensor in *S. cerevisiae*. The experiments were performed with SFmCherry-LL-GCaMP6f-expressing cells incubated in synthetic complete growth media, exciting the fluorescence emitted by the SFmCherry part of the construct (excited with the 543 nm line and collected in the Rch). (*A*) Example of an ACF (*solid line*) and of its corresponding fit (*dashed line*) obtained with Eq. 3, $\chi^2 = 0.003107$. (*B*) Histogram (in frequency) of the diffusion coefficient derived from the fitting parameter, τ_1, with curves that correspond to unimodal (*dashed line*) and bimodal (*solid line*) approximations of the obtained distributions (n = 248).

growth media (*solid line*) and the best fit ($\chi^2 = 0.002022$) of the form of Eq. 4 (*dashed line*). Equation 4 is characterized by two diffusive timescales, τ_1 and τ_2, from which we derived two diffusion coefficients, D_1 and D_2. Attempts to fit the ACF with three diffusive components always converged to having only two distinguishable diffusion coefficients. We show in Fig. 2, *B* and *C* frequency histograms of D_1 and D_2, respectively, obtained from 185 fits. The mean values and corresponding mean ± SE over all the fitted parameters were $D_1 = (9 \pm 1)\ \mu m^2/s$ and $D_2 = (305 \pm 12)\ \mu m^2/s$. Checking for bimodality, the Ak_D values obtained were 0.2664 for D_1 and 0.0292 for D_2, with mean values and proportions of $D_{1a} = 6\ \mu m^2/s$ (84%), $D_{1b} = 30\ \mu m^2/s$ (16%), $D_{2a} = 271\ \mu m^2/s$ (92%), and $D_{2b} = 698\ \mu m^2/s$ (8%).

We then repeated the experiments in cells incubated in synthetic complete growth media supplemented with 200 mM $CaCl_2$ so as to change the equilibrium between intracellular Ca^{2+}, the sensor, and the Ca^{2+} buffers. Also, in this case, we used Eq. 4 to fit the corresponding ACFs. We show in Fig. 3 histograms (in frequency) of the coefficients, D_1 and D_2, derived in this case. The mean values and corresponding mean ± SE were $D_1 = (27 \pm 3)\ \mu m^2/s$ and $D_2 = (374 \pm 33)\ \mu m^2/s$. The Ak_D values obtained were positive, 0.0451 and 0.0192 for D_1 and D_2, indicating bimodality. The mean values and proportion of each population were $D_{1a} = 9\ \mu m^2/s$ (34%), $D_{1b} = 37\ \mu m^2/s$ (66%), $D_{2a} = 236\ \mu m^2/s$ (63%), and $D_{2b} = 605\ \mu m^2/s$ (37%).

The mean value obtained for D_1 in experiments performed in cells with basal cytosolic Ca^{2+} levels (BC) and D_{1a} for the measurements performed in cells with higher levels of cytosolic Ca^{2+} (HC) are consistent with the diffusion coefficient derived for the sensor, $D = (8 \pm 5)\ \mu m^2/s$. The mean values derived for the two populations of D_2 in each set of experiments, with basal or high cytosolic Ca^{2+} levels, are similar but with different proportions and could correspond to effective coefficients.

FCS experiments in *X. laevis* oocytes

In this section, we present the results of FCS experiments performed in *X. laevis* oocytes. These oocytes are a well-known model system in which Ca^{2+} can be observed microinjecting the cells with solutions of the sensor of choice. The basal conditions can also be modified in a controlled manner, including different compounds in the microinjection mix. The experiments were done using the SW Ca^{2+} sensor, Fluo8, whose fluorescence intensity increases over 100 times when bound to Ca^{2+}. In some experiments, the Ca^{2+} chelator EGTA was also added to the cells. To obtain an independent estimation of the free diffusion coefficient of Fluo8, we performed experiments in aqueous solutions (see Fig. S2).

We show in Fig. 4 *A* the example of an ACF obtained in a *X. laevis* oocyte microinjected with a solution containing 100 μM Fluo8 and no added EGTA (*solid line*) and the corresponding best fit ($\chi^2 = 0.0002215$), which was obtained using Eq. 4 (*dashed line*). Two diffusion coefficients, D_1 and D_2, were derived from the fits. As in the experiments in *S. cerevisiae*, attempts to fit the ACFs with three diffusive components gave only two distinguishable diffusion coefficients. We show in Fig. 4, *B* and *C* histograms (in frequency) of the values obtained for the two coefficients over 107 experiments. The average values and mean ± SE for these distributions were $D_1 = (24 \pm 1)\ \mu m^2/s$ and $D_2 = (434 \pm 14)\ \mu m^2/s$, respectively. The Ak_D was positive in both cases, 0.0445 and 0.008, for D_1 and D_2, respectively. In particular, we obtained for D_1, $D_{1a} = 15\ \mu m^2/s$ and $D_{1b} = 36\ \mu m^2/s$ with proportions 56 and 44%, and for D_2, $D_{2a} = 372\ \mu m^2/s$ and $D_{2b} = 644\ \mu m^2/s$, with proportions 77 and 23%.

We then repeated the experiments adding EGTA to the microinjection mix for two different concentrations of the dye (low 100 μM and high 1 mM; final values in the cytosol, low ~3.7 μM and high ~37 μM). The ACFs obtained were then fitted with Eq. 5, from which we could derive three distinguishable diffusion coefficients, D_1, D_2, and D_3. We show in Fig. 5, *A* and *B*, with symbols, the three coefficients derived from the fits as functions of the EGTA concentration used in the mix. We also show, with curves, the four coefficients that, according to the theory, characterize the ACF in the case of a reaction-diffusion system with Ca^{2+}, Fluo8, and EGTA (see Materials and methods; Supporting materials and methods). Three of these coefficients are effective

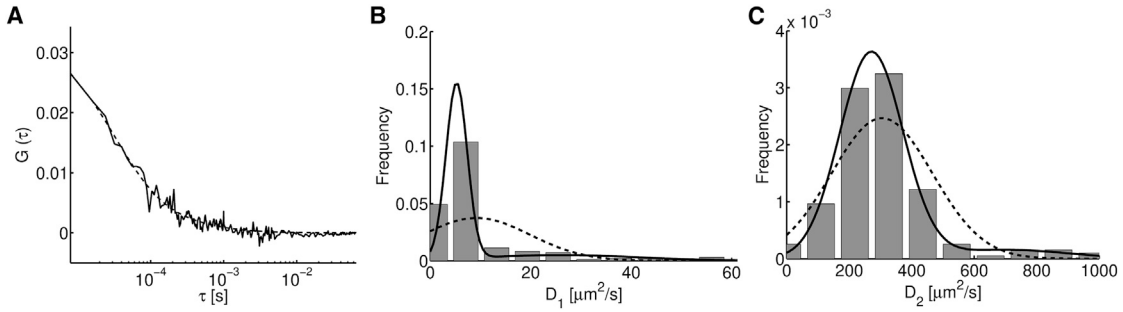

FIGURE 2 FCS experiments in SFmCherry-LL-GCaMP6f-expressing *S. cerevisiae* cells incubated in synthetic complete growth media collecting the fluorescence emitted by GCaMP6f (Gch). (*A*) Example of an ACF (*solid line*) and of its corresponding fit (*dashed line*) obtained with Eq. 4, $\chi^2 = 0.002022$. (*B* and *C*) Histograms (in frequency) of each of the two coefficients derived from the fitting parameters, with curves that correspond to unimodal (*dashed line*) and bimodal (*solid line*) approximations of the obtained distributions (n = 185).

ones (depicted with red, blue, and green), and the fourth one corresponds to the free coefficient of the dye, D_{Fluo8}. We computed them as explained in Materials and methods using the parameters of Table 1 and the same basal cytosolic Ca^{2+} concentration with or without EGTA (the rationale for it being that cells have various mechanisms to keep basal Ca^{2+} constant). The free diffusion coefficients shown in Table 1 actually correspond to values in aqueous solution. We rescaled them by the ratio between an estimate of D_{Ca} in the cytosol ($D_{Ca}^{(cyt)}$) and its value in aqueous solution, $D_{Ca}^{aq} = 760\ \mu m^2/s$, to compute the theoretical curves. In Fig. 5 *A*, we set $D_{Ca}^{(cyt)}$ equal to the largest fitted coefficient derived from the experiments with the largest [EGTA] ($D = 425\ \mu m^2/s$). In Fig. 5 *B*, we set $D_{Ca}^{(cyt)}$ equal to the average of the largest coefficients derived from the fits with all [EGTA] values ($D = 365\ \mu m^2/s$). The reason for this second choice is that, for these [EGTA] values, the largest effective coefficient given by the simple Fluo8-Ca^{2+}-EGTA reaction-diffusion model (red curve) is already indistinguishable from D_{Ca}. It is possible that this is not the case for the actual system probed experimentally, given the simplicity of the model, the variability of the experimental points (diamonds), and that the estimate, $D_{Ca}^{(cyt)}$, derived from the data in Fig. 5 *A* is ~16% larger than the average of the values in Fig. 5 *B*. If we use the same rescaling factor in Fig. 5 *B* as in Fig. 5 *A*, we obtain approximately the same figure, with the only difference being that the values along the theoretical curves are ~16% larger than in the one shown here. This does not change the conclusions that we derive from this figure. Another possible reason for the differences between the theoretical curves and the experimental points is that variations in the cytosolic buffer composition of different cells or regions can lead to changes in the resulting effective diffusion coefficients. To scale out these variations, we show in Fig. 5, *C* and *D*, with symbols, the ratios between the coefficients obtained experimentally at each [EGTA] and the largest coefficient derived from the fits at the same [EGTA] value. Equivalently, for the theoretical curves, we plot the ratio between each coefficient and the largest effective one for each [EGTA]. The values derived directly from the fitting parameters can be seen in Table 2.

DISCUSSION

The rate of Ca^{2+} diffusion is key to determine the cell responses that Ca^{2+} signals can elicit (1). Diffusion in dilute solutions is produced by the same processes that determine the viscosity of the medium, and the diffusion and viscosity coefficients are inversely proportional to one another (13). In such a case, the mean-square displacement of the particles over a time, t, is proportional to Dt, with D, the (free) diffusion coefficient of the particles. Diffusion in the intracellular medium does not always proceed as in dilute solutions, being affected by factors such as molecular crowding and cellular structure. In the case of Ca^{2+}, the displacement of its ions is also affected by the binding/unbinding to/from different cell components generically called buffers. Thus, when moving across regions of approximately uniform buffer concentrations, after a transient, the mean-square displacement of the ions is proportional to $\tilde{D}t$ with $\tilde{D}$, an effective diffusion coefficient that depends on the concentration of Ca^{2+} and of the species it reacts with. $\tilde{D} \rightarrow D$ as $[Ca^{2+}]$ increases, and the buffers become saturated (16,17). Knowing the range of values over which the Ca^{2+} diffusion rate can vary, particularly its highest (free diffusion) end, is key for a comprehensive understanding of the signals. In this work, we have built upon our previous theoretical and experimental works in aqueous solutions (48–50) to quantify the Ca^{2+} diffusion coefficient directly in intact living cells using FCS. As reflected in Figs. 1, 2, 3, and 4, the coefficients estimated with the experiments can vary quite noticeably between cell regions and cells that are subjected to the same conditions. As discussed in what follows, the variability can be due to differences in intracellular viscosity (which affect both free and effective coefficients) or to buffer composition (which not only affects the values that the effective coefficients take on but also which coefficients can be estimated with the experiments).

In this article, we have presented the results obtained in two cell types, *X. laevis* oocytes and cells of *S. cerevisiae*,

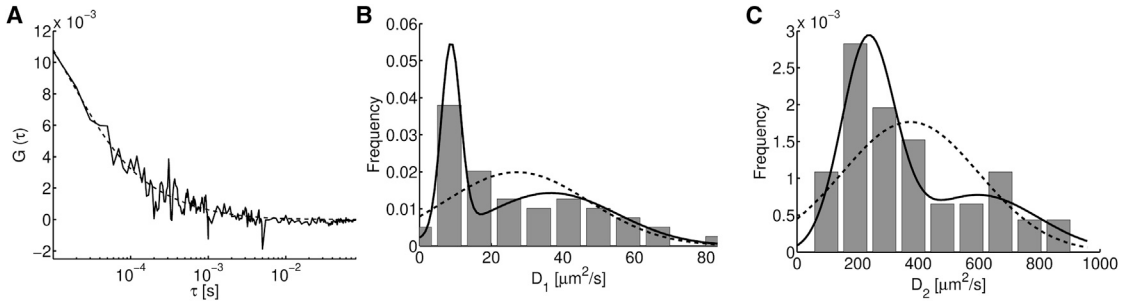

FIGURE 3 FCS experiments in SFmCherry-GCaMP6f-expressing *S. cerevisiae* cells incubated in synthetic complete growth media supplemented with 200 mM $CaCl_2$ collecting the fluorescence emitted by GCaMP6f. (*A*) Example of an ACF (*solid line*) and of its corresponding fit (*dashed line*) obtained with Eq. 4, $\chi^2 = 0.001144$. (*B* and *C*) Histograms (in frequency) of the diffusion coefficients derived, with curves that correspond to unimodal (*dashed line*) and bimodal (*solid line*) approximations of the obtained distributions (n = 49).

in different conditions. A summary of the diffusion coefficients derived from the experiments is given in Table 2 (corresponding to the experiments of Fig. 5 that were performed in oocytes injected with Fluo8 and EGTA) and Table 3 (corresponding to the experiments of Figs. 1, 2, 3, and 4 that were performed, respectively, in *S. cerevisiae* observing the emission in the *red* and *green channels (Rch and Gch)*, repeating the latter with a high [Ca^{2+}] bath and in oocytes injected solely with Fluo8). The experiments of Fig. 5 and Table 2 illustrate how the values that the effective coefficients take on and the coefficients that can be estimated with the experiments vary with buffer composition, providing additional support to our interpretation of the results of Figs. 2, 3, and 4. The ACFs of the experiments of Fig. 5 were fitted with Eq. 5 because three distinguishable diffusion coefficients (D_1, D_2, and D_3) could be derived. The main results of the article are contained in Table 3, where each row corresponds to the estimates derived from the analysis of many records obtained under the same condition. The ACFs of the experiments of Fig. 1 (first row in Table 3) were fitted with Eq. 3 because, as expected, they were characterized by a single diffusive component with coefficient D_1. Those of Figs. 2, 3, and 4 (rows 2–4 of Table 3) were fitted with Eq. 4 because the use of Eq. 5 yielded, in almost all cases, two coefficients that were indistiguinshable between themselves. This occurs even if the actual underlying dynamical system is characterized by the diffusive timescales of the various species that Ca^{2+} interacts with. Which of these timescales can be captured in an experiment in which only one fluorescenct species is observed (Ca^{2+}-bound dye) depends on the (spatially local) equilibrium situation that is being probed in each case (50). All the results reported in Table 3 showed a large variability of the coefficients estimated under the same conditions. To account for this variability, which is apparent in the long tails of the histograms of Figs. 1, 2, 3, and 4, we applied the Akaike criterion (60), which determined that they were described better by a bimodal (the superposition of two Gaussians) than by a unimodal (Gaussian) distribution. This is why in Table 3, we report the means over the whole population of each derived coefficient (D_1 and D_2) and over each of the two subpopulations determined by the Akaike criterion (D_{1a}, D_{1b}, D_{2a}, and D_{2b}). We discuss in the following the interpretation of all these results.

The experiments of Fig. 5 (Table 2) were done with enough EGTA so that this buffer could be the "main competitor" with the dye for Ca^{2+}. In this way, a meaningful comparison between the experimental results and the theoretical ones obtained with the simple Ca^{2+}-dye-EGTA model described in the Supporting materials and methods could be done. Thus, varying [EGTA], we can analyze whether the experimentally derived coefficients are free or effective and to what extent the latter differ from the free ones. Comparing the second largest coefficient, D_2 (*circles*), obtained in the experiments with low (Fig. 5, *A* and *C*) and high (Fig. 5, *B* and *D*) [Fluo8], we observe that it behaves similarly to the theoretical coefficient, D_{ef1} (*blue curve* in Fig. 5, *A* and *C*) and to D_{ef3} (*green curve* in Fig. 5, *B* and *D*). Notice that, with increasing [EGTA], D_{ef1} approaches the EGTA-free diffusion coefficient (227 $\mu m^2/s$, D_{EGTA} from Table 1 rescaled by the factor 0.56, as explained in Results) in Fig. 5 *A* and D_{ef3} approaches the free diffusion of Fluo8 (48 $\mu m^2/s$, D_{Fluo8} from Table 1 rescaled by the factor 0.48 or 56 $\mu m^2/s$ if the rescaling factor, 0.56, is used) in Fig. 5 *B*. This indicates that the set of diffusive timescales that are obtained with the experiments changes depending on the competition between the buffers and the dye, probably because the weight with which they contribute to the ACF also depends on this competition and thus are more or less detectable by the fitting procedure. This occurs on top of the dependence of each effective coefficient with the concentrations (e.g., the dependence with [EGTA] in Fig. 5). Thus, buffer composition affects both the values that the effective coefficients take on and which coefficients can be estimated with the experiments. This highlights the two main problems for the interpretation of the results of Table 3: 1) how to identify the coefficients derived from the fits with those of the actual system and 2) whether the fitted coefficients correspond to free or effective diffusion coefficients. The experiments of Fig. 5 allow us to obtain a

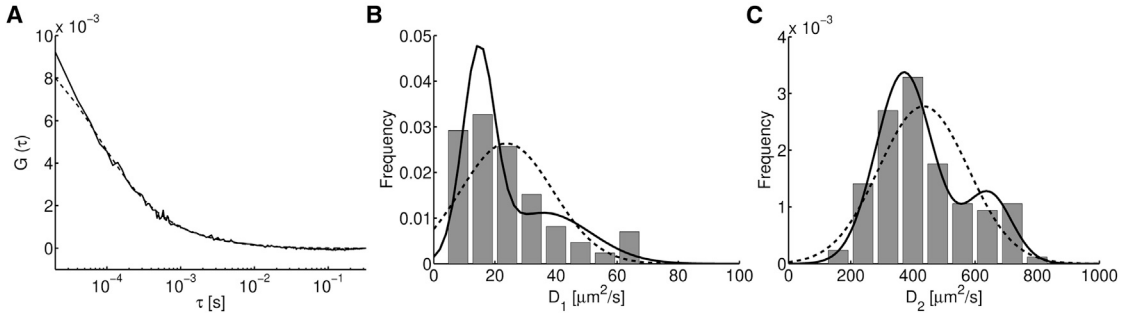

FIGURE 4 FCS experiments in *X. laevis* oocytes microinjected with the Ca^{2+} sensor, Fluo8. The microinjection solution contained 100 μM of Fluo8 and no added EGTA. (*A*) Example of an ACF (*solid line*) and of its corresponding fit (*dashed line*) obtained with Eq. 4, $\chi^2 = 0.0002215$. (*B* and *C*) Histograms (in frequency) of each of the two coefficients derived from the fitting parameters, with curves that correspond to unimodal (*dashed line*) and bimodal (*solid line*) approximations of the obtained distributions (n = 107).

consistent interpretation of the largest coefficient, D_2, derived in the experiments of Fig. 4. The competing effects between the dye and the Ca^{2+} buffers can vary from cell to cell and between regions of a cell. Differences in buffer composition can then be the cause for the large variability of the experimentally derived coefficients of Table 3. As discussed in what follows, this is not the only source of variability.

The largest experimentally determined coefficient of Fig. 5 *A*, D_3 (*diamonds*), increases with [EGTA] as the largest effective coefficient of the theoretical model, D_{ef2}. With increasing [EGTA], D_{ef2} approaches the free Ca^{2+} diffusion coefficient D_{Ca}, which is the largest coefficient of the problem. We could thus consider that the value $D_3 = (425 \pm 18)$ $\mu m^2/s$, obtained for the largest [EGTA] in these experiments (see Table 2), is an estimate of D_{Ca} in the cytosol of oocytes. How do we reconcile this estimate with the fact that the largest coefficient derived from the experiments performed in oocytes with no EGTA (see Fig. 4 *C*) was much bigger in a significant fraction of the experiments? As mentioned before, the histogram of Fig. 4 *C* is best approximated by a bimodal distribution with subpopulations of means, 372 and 644 $\mu m^2/s$, embracing 77 and 23% of the data (see fourth row in Table 3). This variability is much larger than the one that changes in buffer composition cause on the largest determined coefficient of Fig. 5. Namely, the experimental coefficient, D_3, stays close to the theoretical one, D_{ef2}, which differs by less than ~15% with respect to the free coefficient, D_{Ca}, for all the concentrations, [EGTA], and the two dye concentrations probed in the experiments of Fig. 5. Assuming that the Stokes-Einstein relation between viscosity and diffusivity holds, we can associate the variability of D_2 in Fig. 4 *C* mostly to changes in viscosity, which, as already mentioned, would imply changes in the value of the free diffusion coefficients. Given that $D_{Ca} = 760$ $\mu m^2/s$ in aqueous solutions (61), if we consider that the values 372 and 644 $\mu m^2/s$ are within 15% of D_{Ca} in different regions of the cytosol, we then conclude that cytosolic viscosity could approximately vary between 2 and 1.2 times that of water. This variability, $1.2/2 \sim 0.6$, is consistent with the one observed in the results derived from the experiments in yeast in which the emission coming from the SFmCherry part of the sensor was analyzed (first row in Table 3). Namely, we observe that the set of values obtained for the diffusion coefficient, D_1, which should correspond to the free diffusion coefficient of the sensor protein, can also be divided in two populations with means 12 and 7 $\mu m^2/s$, whose ratio is $7/12 \sim 0.6$. Viscosity variability could then explain the wide, nonsymmetric distribution of the largest diffusion coefficient obtained in the experiments of Fig. 4. The results of Fig. 5 *A* were obtained over fewer experiments than those of Fig. 4. Thus, it is more likely that they correspond to values D_{Ca} within the subpopulation of Fig. 4 *C* of larger probability, i.e., the one with mean, 372 $\mu m^2/s$. As shown in the Supporting materials and methods, the estimate, 372 $\mu m^2/s$, falls very close to the theoretical curve D_{ef3} of Fig. 5 *A* (*red line*), which approaches $D_{Ca} = (425 \pm 18)$ $\mu m^2/s$ with increasing [EGTA]. This provides further support to the conclusion that the experimentally determined coefficient, D_2, of Fig. 4 (fourth row in Table 3) is very close (within ~15%) to the free Ca^{2+} diffusion coefficient in the cytosol, and the variability among the estimated values, particularly between the means of each subpopulation, is mostly due to changes in cytosolic viscosity. It is important to note that the means over both populations are larger than the estimate, $D_{Ca} = 220$ $\mu m^2/s$, of Allbritton et al. (16). It has been observed that the cytosol is a complex liquid that is not characterized by a single viscosity (62–66), with "sensed" values that depend on the size of the diffusive particles, which, for small ones, vary between ~1.3 and 3 times the viscosity of water (65), similar to the 1.2–2 range that we derived from our experiments. Our results are also consistent with those of Rienzo et al. (68), which revealed that, in the cytosol, molecules diffuse freely with a coefficient as the one in a dilute solution at short scales.

A large variability is also observed among the values of the largest coefficient, D_2, derived from the two types of experiments performed in *S. cerevisiae* in which the emission from the GCaMP6f part of the sensor was excited (Gch) (Figs. 2 and 3). The D_2 variability in Figs. 2 *C* and 3 *C*,

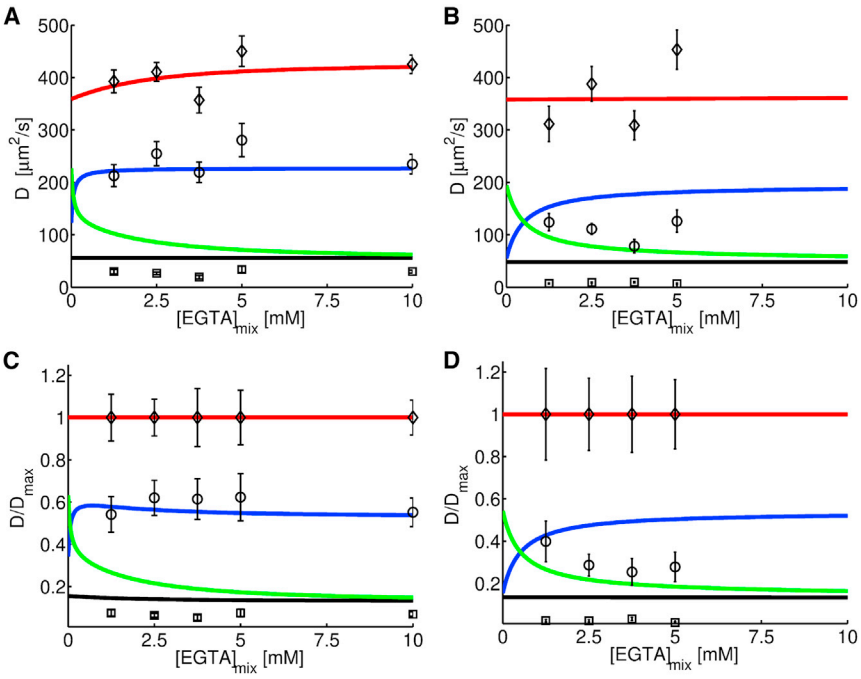

FIGURE 5 Diffusion coefficients derived from experiments performed in oocytes with EGTA and Fluo8 and theoretical results obtained for a reaction-diffusion system with Ca^{2+}, EGTA, and Fluo8. (*A*) and (*C*) correspond to experiments with [Fluo8] = 100 μM in the mix and (*B*) and (*D*) to [Fluo8] = 1000 μM in the mix. In all cases, the ACFs were fitted with Eq. 5, from which three diffusion coefficients, $D_1 < D_2 < D_3$, were derived (shown with *symbols*). The theoretical computations (shown with *solid lines*) were done using the parameters of Table 1. In (*A*) and (*B*), the theoretical results (D_{Fluo8}, D_{ef1}, D_{ef2}, and D_{ef3}, in *black*, *blue*, *red*, and *green*, respectively) were rescaled by the factors 0.56 in (*A*) and 0.48 in (*B*), which we estimated as the ratio between D_{Ca} in the cytosol and in aqueous solutions (see main text). In (*C*) and (*D*), we show the ratios between the coefficients and one of them, D_{max}, at each [EGTA]. For the theoretical curves, D_{max} is the largest effective coefficient for the concentrations probed, D_{ef2} (*black*: D_{Fluo8}/D_{ef2}, *blue*: D_{ef1}/D_{ef2}, *green*: D_{ef3}/D_{ef2}), and for the experimental ones, it is the largest fitted one, D_3 (*squares*: D_1/D_3, *circles*: D_2/D_3). For a reference, we also include D_3/D_3 (*diamonds*) and D_{ef2}/D_{ef2} (*red curve*). For the numerical computations, we used [Fluo8] = 3.7 and 37 μM for low and high Fluo8, respectively. Symbols represent mean values and error bars the mean ± SE. To see the figure in color, go online.

however, is slightly smaller than in Fig. 4 *C*. It is also smaller than the D_1 variability observed in the experiments in which the fluorescence was collected in the Rch (Fig. 1 *B*), which is due to changes in cytosolic viscosity. The latter is reflected in that the ratio between the means over each population into which the values, D_2, can be divided is $D_{2a}/D_{2b} \sim 0.39$ and $D_{2a}/D_{2b} \sim 0.39$ for the Gch/BC and Gch/HC experiments, respectively, whereas it is $D_{1a}/D_{1b} \sim 0.6$ in the Rch experiments (Table 3). This is an indication that the coefficient, D_2, obtained in the Gch experiments performed in *S. cerevisiae* might correspond to an effective coefficient that is further apart from D_{Ca} than in the experiments performed in oocytes. This is consistent with the observation that the means over each subpopulation, D_{2a} and D_{2b}, decrease with increasing Ca^{2+} (see Table 3), a behavior that has been observed in the largest coefficient derived in the experiments performed in aqueous solutions presented in Fig. 7 of Villarruel and Dawson (50). The means, D_{2b}, over the subpopulations with the largest values obtained in the Gch/BC and Gch/HC experiments in *S. cerevisiae* (698 and 605 $\mu m^2/s$, respectively), differ by less than 10% with respect to the value obtained in oocytes, $D_{2b} = 644$ $\mu m^2/s$. The means, D_{2a}, over the subpopulations with the lowest values, on the other hand (271 and 236 $\mu m^2/s$ for Gch/BC and Gch/HC, respectively), differ by ~30% with respect to the value obtained in oocytes, $D_{2a} = 372$ $\mu m^2/s$. It seems as if the highest end of the D_2 distribution in *S. cerevisiae* is closer to D_{Ca} than the lowest one. This observation can be explained if we assume that the buffer composition in *S. cerevisiae* is such that the largest experimentally estimated coefficient corresponds to a different effective coefficient depending on the probed region of the cytosol (as illustrated by the transition observed in the second largest coefficient between Fig. 5, *A* and *B*). This is consistent with the fact that, when increasing Ca^{2+} in the bath, the means, D_{2a} and D_{2b}, do not vary as much as the relative probability of obtaining a diffusion coefficient within each subpopulation (the relative weights). This marked change in the relative weights can also be reflecting that it is not only the cytosolic Ca^{2+} concentration that changes between the experiments with low and high Ca^{2+} bath but also the internal state of the cell (55). Another possibility is that these subpopulations can still

TABLE 2 Diffusion coefficients derived from the ACFs obtained in the experiments performed in oocytes with EGTA and two concentrations of [Fluo8]

	$[EGTA]_{mix}$	D_1	D_2	D_3
Low [Fluo8] (Fig. 5, *A* and *C*)	1.25	30 ± 4	213 ± 21	393 ± 22
	2.5	26 ± 3	255 ± 23	411 ± 18
	3.75	19 ± 3	219 ± 19	357 ± 24
	5	34 ± 6	280 ± 32	450 ± 29
	10	30 ± 3	235 ± 19	425 ± 18
High [Fluo8] (Fig. 5, *B* and *D*)	1.25	7 ± 1	124 ± 17	311 ± 34
	2.5	9 ± 1	111 ± 10	388 ± 33
	3.75	9 ± 1	78 ± 13	309 ± 28
	5	7 ± 1	126 ± 21	453 ± 37

Diffusion coefficients are expressed in $\mu m^2/s$, and [EGTA] is expressed in mM. Diffusion coefficients are illustrated in Fig. 5.

TABLE 3 Diffusion coefficients derived from the FCS experiments performed in *S. cerevisiae* cells, observing the fluorescence emitted by the SFmCherry (Rch) or the GCaMP6f (Gch) part of the fluorophore, as indicated, in basal (BC) or high (HC) Ca^{2+} media and in *X. laevis* oocytes with no EGTA

		D_1	D_{1a}	D_{1b}	D_2	D_{2a}	D_{2b}	N	Figure
S. cerevisiae	Rch	8 ± 0.25	7 (70%)	12 (30%)	–	–	–	248	Fig. 1
	Gch/BC	9 ± 1	6 (84%)	30 (16%)	305 ± 12	271 (92%)	698 (8%)	185	Fig. 2
	Gch/HC	27 ± 3	9 (34%)	37 (66%)	374 ± 33	236 (63%)	605 (37%)	49	Fig. 3
X. laevis		24 ± 1	15 (56%)	36 (44%)	434 ± 14	372 (77%)	644 (23%)	107	Fig. 4

The diffusion coefficients are expressed in $\mu m^2/s$ as mean value ± SE for D_1 and D_2 or mean value (proportion of distribution) for D_{1a}, D_{1b}, D_{2a}, and D_{2b}.

be split once more, something that we will explore in future works.

We now analyze the smallest coefficient, D_1, derived from the experiments in oocytes and the ones in yeast observed in the Gch. For the latter, both in the cases of basal (BC) or high (HC) Ca^{2+} media, the set of D_1 values can be grouped in two subpopulations using the Akaike criterion. The means of one subpopulation (D_{1a}, Gch/BC and Gch/HC in Table 3) are similar to the free diffusion of the sensor estimated from the observations in the Rch, 6–9 $\mu m^2/s$ (D_1 or D_{1a}, Rch, in Table 3). This gives a further validation to the estimate we obtained of the free sensor diffusion coefficient. The mean and the proportion of the other subpopulation, D_{1b}, increase with $[Ca^{2+}]$ (compare the BC and the HC cases in Table 3). Thus, D_{1b} most likely corresponds to an effective coefficient that is a concentration-dependent weighted average of the free coefficients of buffers, fluorophore, and Ca^{2+}. In the case of *X. laevis* oocytes, the values, D_1, derived from the fittings can be grouped into two subpopulations following the Akaike criterion as well. 56% of the data corresponded to a distribution centered around 15 $\mu m^2/s$ and the other 44% to a distribution centered around 36 $\mu m^2/s$ (Table 3). Given the results of Fig. 5 (see also Table 2), we can interpret these coefficients as effective ones that depend on the free coefficient of the dye (D_{Fluo8} ~50–60 $\mu m^2/s$ in the cytosol using the conversion factor from aqueous solution derived from Fig. 5, *A* and *B*) and on the coefficients of slower or immobile Ca^{2+} buffers.

Summarizing, the experiments performed in *X. laevis* oocytes and in *S. cerevisiae* that we have presented in this work show that the free diffusion coefficient of Ca^{2+} in the cytosol of living cells, D_{Ca}, is typically larger than previously assumed (~220 $\mu m^2/s$) and that it can vary over a very wide range of values in a similar way as has been observed for the cytoplasmic viscosity. Given the experiments performed in oocytes for which we have a better indication that one of the derived coefficients is close enough to D_{Ca}, we conclude that D_{Ca} varies around ~400 $\mu m^2/s$ in most cases. There are certain instances, however, at which the Ca^{2+} cytosolic free diffusion can occur at approximately the same rate as in dilute aqueous solutions, ~650 $\mu m^2/s$. The implications of the latter for signaling will depend on the lengthscale over which such a high diffusion rate could be maintained. Further studies are necessary to analyze this aspect.

SUPPORTING MATERIAL

Supporting material can be found online at https://doi.org/10.1016/j.bpj.2021.08.019.

AUTHOR CONTRIBUTIONS

S.P.D. and C.V. participated in the oocytes experimental design and data interpretation. P.S.A. and C.V. participated in the yeast experimental design and data interpretation. C.V. performed the experiments and analyzed the data. S.P.D. supervised the project. C.V. and S.P.D. wrote the manuscript. All authors discussed the results and contributed to the final manuscript.

ACKNOWLEDGMENTS

We thank Dr. Sivaraj Sivaramakrishnan who provided the long linker sequence, Dr. Gabriela Amodeo who provided the *X. laevis* oocytes, Nahuel Tarkowski for help with some yeast experiments, and Dr. Lorena Sigaut for help with Förster resonance energy transfer efficiency experiments.

This research has been supported by Universidad de Buenos Aires (UBACyT 20020170100482BA) and Agencia Nacional de Promoción Científica y Tecnológica (PICT 2015-3824 and PICT 2018-02026 to S.P.D. and PICT 2017-0854 to P.S.A.). P.S.A. and S.P.D. are members of Carrera del Investigador Científico.

REFERENCES

1. Berridge, M. J., M. D. Bootman, and P. Lipp. 1998. Calcium–a life and death signal. *Nature.* 395:645–648.
2. Wei, C., X. Wang, …, H. Cheng. 2009. Calcium flickers steer cell migration. *Nature.* 457:901–905.
3. Thurley, K., S. C. Tovey, …, M. Falcke. 2014. Reliable encoding of stimulus intensities within random sequences of intracellular Ca2+ spikes. *Sci. Signal.* 7:ra59.
4. Kniss-James, A. S., C. A. Rivet, …, M. L. Kemp. 2017. Single-cell resolution of intracellular T cell Ca^{2+} dynamics in response to frequency-based H_2O_2 stimulation. *Integr. Biol.* 9:238–247.
5. Hunt, H., A. Tilūnaitė, …, E. J. Crampin. 2020. Ca^{2+} release via IP_3 receptors shapes the cardiac Ca^{2+} transient for hypertrophic signaling. *Biophys. J.* 119:1178–1192.
6. Rizzuto, R., D. De Stefani, …, C. Mammucari. 2012. Mitochondria as sensors and regulators of calcium signalling. *Nat. Rev. Mol. Cell Biol.* 13:566–578.
7. Cui, J., J. A. Kaandorp, …, M. V. Filatov. 2009. Calcium homeostasis and signaling in yeast cells and cardiac myocytes. *FEMS Yeast Res.* 9:1137–1147.
8. Lange, M., and E. Peiter. 2020. Calcium transport proteins in fungi: the phylogenetic diversity of their relevance for growth, virulence, and stress resistance. *Front. Microbiol.* 10:3100.

9. Schwaller, B. 2010. Cytosolic Ca2+ buffers. *Cold Spring Harb. Perspect. Biol.* 2:a004051.
10. Dargan, S. L., B. Schwaller, and I. Parker. 2004. Spatiotemporal patterning of IP3-mediated Ca2+ signals in Xenopus oocytes by Ca2+-binding proteins. *J. Physiol.* 556:447–461.
11. Fraiman, D., and S. P. Dawson. 2014. Buffer regulation of calcium puff sequences. *Phys. Biol.* 11:016007.
12. Piegari, E., L. F. Lopez, and S. Ponce Dawson. 2018. Using two dyes to observe the competition of Ca^{2+} trapping mechanisms and their effect on intracellular Ca^{2+} signals. *Phys. Biol.* 15:066006.
13. Einstein, A. 1989. The Collected Papers of Albert Einstein, Volume 2, Translated by Anna Beck, consultant Peter Havas. Princeton University Press, Princeton, NJ.
14. Berg, H. C. 1993. Random Walks in Biology. Princeton University Press, Princeton, NJ.
15. Naraghi, M., and E. Neher. 1997. Linearized buffered Ca2+ diffusion in microdomains and its implications for calculation of [Ca2+] at the mouth of a calcium channel. *J. Neurosci.* 17:6961–6973.
16. Allbritton, N. L., T. Meyer, and L. Stryer. 1992. Range of messenger action of calcium ion and inositol 1,4,5-trisphosphate. *Science.* 258:1812–1815.
17. Pando, B., S. P. Dawson, …, J. E. Pearson. 2006. Messages diffuse faster than messengers. *Proc. Natl. Acad. Sci. USA.* 103:5338–5342.
18. Carbó, N., N. Tarkowski, …, P. S. Aguilar. 2017. Sexual pheromone modulates the frequency of cytosolic Ca^{2+} bursts in *Saccharomyces cerevisiae*. *Mol. Biol. Cell.* 28:501–510.
19. Flegg, M. B., S. Rüdiger, and R. Erban. 2013. Diffusive spatio-temporal noise in a first-passage time model for intracellular calcium release. *J. Chem. Phys.* 138:154103.
20. MacDowell, C. J., and T. J. Buschman. 2020. Low-dimensional spatio-temporal dynamics underlie cortex-wide neural activity. *Curr. Biol.* 30:2665–2680.e8.
21. Dawson, S. P., J. Keizer, and J. E. Pearson. 1999. Fire-diffuse-fire model of dynamics of intracellular calcium waves. *Proc. Natl. Acad. Sci. USA.* 96:6060–6063.
22. Voorsluijs, V., S. P. Dawson, …, G. Dupont. 2019. Deterministic limit of intracellular calcium spikes. *Phys. Rev. Lett.* 122:088101.
23. Piegari, E., and S. Ponce Dawson. 2019. Functional Ca^{2+} channels between channel clusters are necessary for the propagation of IP_3R-mediated Ca^{2+} waves. *Math. Comput. Appl.* 24:61.
24. Lock, J. T., and I. Parker. 2020. IP_3 mediated global Ca^{2+} signals arise through two temporally and spatially distinct modes of Ca^{2+} release. *eLife.* 9:e55008.
25. Fujii, Y., S. Maekawa, and M. Morita. 2017. Astrocyte calcium waves propagate proximally by gap junction and distally by extracellular diffusion of ATP released from volume-regulated anion channels. *Sci. Rep.* 7:13115.
26. Denizot, A., M. Arizono, …, H. Berry. 2019. Simulation of calcium signaling in fine astrocytic processes: effect of spatial properties on spontaneous activity. *PLoS Comput. Biol.* 15:e1006795.
27. Bezprozvanny, I. 2005. The inositol 1,4,5-trisphosphate receptors. *Cell Calcium.* 38:261–272.
28. Foskett, J. K., C. White, …, D. O. Mak. 2007. Inositol trisphosphate receptor Ca2+ release channels. *Physiol. Rev.* 87:593–658.
29. Taylor, C. W., and S. C. Tovey. 2010. IP(3) receptors: toward understanding their activation. *Cold Spring Harb. Perspect. Biol.* 2:a004010.
30. Fabiato, A. 1983. Calcium-induced release of calcium from the cardiac sarcoplasmic reticulum. *Am. J. Physiol.* 245:C1–C14.
31. Dickinson, G. D., K. L. Ellefsen, …, I. Parker. 2016. Hindered cytoplasmic diffusion of inositol trisphosphate restricts its cellular range of action. *Sci. Signal.* 9:ra108.
32. Denis, V., and M. S. Cyert. 2002. Internal Ca(2+) release in yeast is triggered by hypertonic shock and mediated by a TRP channel homologue. *J. Cell Biol.* 156:29–34.
33. Viladevall, L., R. Serrano, …, J. Ariño. 2004. Characterization of the calcium-mediated response to alkaline stress in *Saccharomyces cerevisiae*. *J. Biol. Chem.* 279:43614–43624.
34. Cunningham, K. W. 2011. Acidic calcium stores of Saccharomyces cerevisiae. *Cell Calcium.* 50:129–138.
35. Cyert, M. S., and C. C. Philpott. 2013. Regulation of cation balance in *Saccharomyces cerevisiae*. *Genetics.* 193:677–713.
36. Santamaria, F., S. Wils, …, G. J. Augustine. 2006. Anomalous diffusion in Purkinje cell dendrites caused by spines. *Neuron.* 52:635–648.
37. Biess, A., E. Korkotian, and D. Holcman. 2011. Barriers to diffusion in dendrites and estimation of calcium spread following synaptic inputs. *PLoS Comput. Biol.* 7:e1002182.
38. Ventura, A. C., L. Bruno, …, S. P. Dawson. 2005. A model-independent algorithm to derive Ca2+ fluxes underlying local cytosolic Ca2+ transients. *Biophys. J.* 88:2403–2421.
39. Bruno, L., G. Solovey, …, S. P. Dawson. 2010. Quantifying calcium fluxes underlying calcium puffs in *Xenopus laevis* oocytes. *Cell Calcium.* 47:273–286.
40. Piegari, E., L. Lopez, …, S. Ponce Dawson. 2014. Fluorescence fluctuations and equivalence classes of Ca^{2+} imaging experiments. *PLoS One.* 9:e95860.
41. Magde, D., E. Elson, and W. W. Webb. 1972. Thermodynamic fluctuations in a reacting system—measurement by fluorescence correlation spectroscopy. *Phys. Rev. Lett.* 29:705–708.
42. Haustein, E., and P. Schwille. 2007. Fluorescence correlation spectroscopy: novel variations of an established technique. *Annu. Rev. Biophys. Biomol. Struct.* 36:151–169.
43. Abu-Arish, A., A. Porcher, …, C. Fradin. 2010. High mobility of bicoid captured by fluorescence correlation spectroscopy: implication for the rapid establishment of its gradient. *Biophys. J.* 99:L33–L35.
44. Gupta, A., I. Y. Phang, and T. Wohland. 2020. To hop or not to hop: exceptions in the FCS diffusion law. *Biophys. J.* 118:2434–2447.
45. Paredes, R. M., J. C. Etzler, …, J. D. Lechleiter. 2008. Chemical calcium indicators. *Methods.* 46:143–151.
46. Mank, M., and O. Griesbeck. 2008. Genetically encoded calcium indicators. *Chem. Rev.* 108:1550–1564.
47. Piegari, E., L. Sigaut, and S. Ponce Dawson. 2015. Ca^{2+} images obtained in different experimental conditions shed light on the spatial distribution of IP_3 receptors that underlie Ca^{2+} puffs. *Cell Calcium.* 57:109–119.
48. Sigaut, L., C. Villarruel, …, S. Ponce Dawson. 2017. Fluorescence correlation spectroscopy experiments to quantify free diffusion coefficients in reaction-diffusion systems: the case of Ca∧2+ and its dyes. *Phys. Rev. E.* 95:062408.
49. Sigaut, L., C. Villarruel, and S. Ponce Dawson. 2017. FCS experiments to quantify Ca^{2+} diffusion and its interaction with buffers. *J. Chem. Phys.* 146:104203.
50. Villarruel, C., and S. P. Dawson. 2020. Quantification of fluctuations from fluorescence correlation spectroscopy experiments in reaction-diffusion systems. *Phys. Rev. E.* 102:052407.
51. van den Ent, F., and J. Löwe. 2006. RF cloning: a restriction-free method for inserting target genes into plasmids. *J. Biochem. Biophys. Methods.* 67:67–74.
52. Sivaramakrishnan, S., and J. A. Spudich. 2011. Systematic control of protein interaction using a modular ER/K α-helix linker. *Proc. Natl. Acad. Sci. USA.* 108:20467–20472.
53. Swanson, C. J., and S. Sivaramakrishnan. 2014. Harnessing the unique structural properties of isolated α-helices. *J. Biol. Chem.* 289:25460–25467.
54. Cho, J.-H., C. J. Swanson, …, R. H. Chow. 2017. The GCaMP-R family of genetically encoded ratiometric calcium indicators. *ACS Chem. Biol.* 12:1066–1074.
55. Cai, L., C. K. Dalal, and M. B. Elowitz. 2008. Frequency-modulated nuclear localization bursts coordinate gene regulation. *Nature.* 455:485–490.

56. Culbertson, C. T., S. C. Jacobson, and J. Michael Ramsey. 2002. Diffusion coefficient measurements in microfluidic devices. *Talanta.* 56:365–373.

57. Gennerich, A., and D. Schild. 2002. Anisotropic diffusion in mitral cell dendrites revealed by fluorescence correlation spectroscopy. *Biophys. J.* 83:510–522.

58. The MathWorks Inc. 2010. MATLAB version 7.10.0 (R2010a). The MathWorks Inc., Natick, MA.

59. Krichevsky, O., and G. Bonnet. 2002. Fluorescence correlation spectroscopy: the technique and its applications. *Rep. Prog. Phys.* 65:251–297.

60. Akaike, H. 1992. Information theory and an extension of the maximum likelihood principle. *In* Breakthroughs in Statistics, Springer Series in Statistics (Perspectives in Statistics). S. Kotz and N. Johnson, eds. Springer US, pp. 199–213.

61. Qin, D. Y., A. Yoshida, and A. Noma. 1991. Limitations due to unstirred layers in measuring channel response of excised membrane patch using rapid solution exchange methods. *Jpn. J. Physiol.* 41:333–339.

62. Blum, J. J., G. Lawler, …, I. Shin. 1989. Effect of cytoskeletal geometry on intracellular diffusion. *Biophys. J.* 56:995–1005.

63. Elowitz, M. B., M. G. Surette, …, S. Leibler. 1999. Protein mobility in the cytoplasm of *Escherichia coli*. *J. Bacteriol.* 181:197–203.

64. Szymański, J., A. Patkowski, …, R. Holyst. 2006. Diffusion and viscosity in a crowded environment: from nano- to macroscale. *J. Phys. Chem. B.* 110:25593–25597.

65. Kalwarczyk, T., N. Zibacz, …, R. Hołyst. 2011. Comparative analysis of viscosity of complex liquids and cytoplasm of mammalian cells at the nanoscale. *Nano Lett.* 11:2157–2163.

66. Sozanski, K., A. Wisniewska, …, R. Holyst. 2016. Motion of molecular probes and viscosity scaling in polyelectrolyte solutions at physiological ionic strength. *PLoS One.* 11:e0161409.

67. Wood, C., J. Huff, …, W. Wiegraebe. 2011. Fluorescence correlation spectroscopy as tool for high-content-screening in yeast (HCS-FCS). *Single Molecule Spectroscopy and Imaging IV, International Society for Optics and Photonics.* 7905:79050H.

68. Di Rienzo, C., V. Piazza, …, F. Cardarelli. 2014. Probing short-range protein Brownian motion in the cytoplasm of living cells. *Nat. Commun.* 5:5891.

Biophysical Journal, Volume *120*

Supplemental information

High rates of calcium-free diffusion in the cytosol of living cells

Cecilia Villarruel, Pablo S. Aguilar, and Silvina Ponce Dawson

SUPPORTING MATERIAL OF HIGH RATES OF CALCIUM FREE DIFFUSION IN THE CYTOSOL OF LIVING CELLS

Cecilia Villarruel, Pablo S. Aguilar, Silvina Ponce Dawson

THEORETICAL CALCULATION OF EFFECTIVE DIFFUSION COEFFICIENTS

We consider the evolution equations of the reaction-diffusion system with Ca^{2+}, a Ca^{2+} sensor, F, and, if present, a Ca^{2+} chelator, E, that react according to Eqs. (8) with $X = F, E$:

$$\begin{aligned}
\frac{\partial [E]_T}{\partial t} &= D_E \nabla^2 [E], \\
\frac{\partial [F]_T}{\partial t} &= D_F \nabla^2 [F], \\
\frac{\partial [CaE]}{\partial t} &= D_E \nabla^2 [CaE] + kon_E [Ca]\ ([E]_T - [CaE]) - koff_E [CaE], \\
\frac{\partial [CaF]}{\partial t} &= D_F \nabla^2 [CaF] + kon_F [Ca]\ ([F]_T - [CaF]) - koff_F [CaF], \\
\frac{\partial [Ca]}{\partial t} &= D_{Ca} \nabla^2 [Ca] - kon_F [Ca]\ ([F]_T - [CaF]) + koff_F [CaF] \\
&- kon_E [Ca]\ ([E]_T - [CaE]) + koff_E [CaE],
\end{aligned} \tag{S1}$$

where $[E]_T = [E] + [CaE]$, $[F]_T = [F] + [CaF]$ at every time and spatial point, and the free diffusion coefficients of the species are: D_{Ca} (for Ca^{2+}), D_E (for E and CaE) and D_F (for F and CaF). For the sensor we use $F = Fluo8$ or $F = GCaMP6f$. To obtain the expected theoretical diffusion coefficients we linearize these equations around the spatially uniform and stationary (equilibrium) solution ($[E]_{tot}$, $[F]_{tot}$, $[CaF]_{eq}$, $[CaE]_{eq}$, $[Ca]_{eq}$), Fourier transform them and derive the 5 eigenvalues, $\lambda_i(q^2)$, of the problem as functions of the (square of the) wavenumber, $\mathbf{q}$, the variable conjugate to the position vector, $\mathbf{r}$, in Fourier space (see Villarruel and Dawson (1) for details). In the presence of the species, E, there are two trivial eigenvalues associated, respectively, to the free diffusion coefficient of the sensor and of the Ca^{2+} chelator:

$$\lambda_4 = -D_F q^2, \tag{S2}$$

$$\lambda_5 = -D_E q^2. \tag{S3}$$

The effective diffusion coefficients, $D_{ef\,i}$, $i = 1, 2, 3$, are derived from the expansion of the other three eigenvalues in powers of q^2 up to $O(q^2)$:

$$\lambda_i \approx -\nu_{ef\,i} - D_{ef\,i} q^2, \quad i = 1, 2, 3. \tag{S4}$$

Among these 3 non-trivial eigenvalues there is one such that $\nu_{ef\,i} = 0$. We label it with the subscript $i = 1$. $D_{ef\,1}$ has a simple analytic expression:

$$D_{ef\,1} = \frac{D_{Ca} + x_F D_F + x_E D_E}{1 + x_F + x_E}, \tag{S5}$$

where $x_F = [F]_{eq}^2/(Kd_F [F]_{tot})$ and $x_E = [E]_{eq}^2/(Kd_E [E]_{tot})$ with $[F]_{eq} = [F]_{tot} - [CaF]_{eq}$ and $[E]_{eq} = [E]_{tot} - [CaE]_{eq}$ the equilibrium concentrations of free dye and chelator, respectively. Assuming that the only fluorescent species is CaF, the ACF of the fluorescence fluctuations depends on λ_i, $i = 1, 2, 3, 4$ but not on λ_5. The analytic expressions of $D_{ef\,2}$, $D_{ef\,3}$, $\nu_{ef\,2}$ and $\nu_{ef\,3}$ are very long (see *e.g.* (2)). $D_{ef\,2}$ and $D_{ef\,3}$ depend on the ratio $k_E = koff_E/koff_F$ and the various quantities satisfy:

$$D_{ef\,1} + D_{ef\,2} + D_{ef\,3} = D_{Ca} + D_F + D_E, \tag{S6}$$

$$\nu_{ef\,2} + \nu_{ef\,3} = \nu_F + \nu_E, \tag{S7}$$

where $\nu_F = koff_F (F_{eq}/Kd_F + F_{tot}/F_{eq})$ and $\nu_E = koff_E (E_{eq}/Kd_E + E_{tot}/E_{eq})$. As explained in Materials and Methods, we compute $D_{ef\,1}$, $D_{ef\,2}$, and $D_{ef\,3}$ using the free diffusion coefficients, D_{Ca}, D_F, D_E, that hold in aqueous solutions. Under the assumption that all the free coefficients vary by the same factor when going from aqueous solutions to the cytosol, then, normalizing $D_{ef\,1}$, $D_{ef\,2}$, and $D_{ef\,3}$ by any of the free coefficients, *e.g.*, D_{Ca}, we obtain quantities that remain the same in the cytosol and in aqueous solutions. Under the same assumption, the ratio between any of the coefficients (effective or free)

for a given set of total concentrations is also the same in the cytosol or in aqueous solutions. These are the quantities that we compare with the experimental results obtained in cells.

One might wonder what is the rationale behind using a relatively simple reaction-diffusion system to interpret the results obtained in settings, like a living cell, where many more species interact with Ca^{2+}. In principle, we expect that the non-fluorescent species, E, of Eqs. (S1) can represent an *effective buffer* that reflects the net effect of the interaction of various intracellular species with Ca^{2+}, particularly, in their competition with the dye for Ca^{2+}. The experimental results performed in oocytes with Fluo8 and EGTA seem to confirm this expectation. Namely, in the presence of a relatively large concentration of the exogenous Ca^{2+} buffer, EGTA, an effective diffusion coefficient that is dominated by the free EGTA diffusion coefficient can be estimated from the experiments (Figure 5, A and C), unless the interaction with the sensor becomes more relevant and an effective coefficient that is dominated by D_{Fluo8} is estimated instead (Figure 5, B and D).

In aqueous solutions, when the non-fluorescent species, E, is absent (*i.e.*, $[E]_T = 0$), the system reduces to the 2nd, 4th and 5th equations in (S1) and the ACF depends on three eigenvalues (3): the one given by Eq. (S2) (associated to the free diffusion coefficient of the sensor) and another two whose small q approximations (Eq. (S4)) have $\nu_{ef1} = 0$ and D_{ef1} given by Eq. (S5) with $x_E = 0$ and

$$D_{ef2} = \frac{x_F D_{Ca} + D_F}{1 + x_F + x_E} \tag{S8}$$

CONSTRUCTION AND OPTIMIZATION OF A DUAL FLUORESCENT GENETICALLY ENCODED Ca^{2+} SENSOR

The quantification of the transport properties (diffusion coefficient and concentration) of the Ca^{2+} sensor is important to derive the free diffusion coefficient of Ca^{2+} from its ACF (Villarruel and Ponce Dawson, 2020). In order to simultaneously register the sensor dynamics and its Ca^{2+}-bound dependent fluorescence in living cells we fused the fluorescent protein super folder monomeric Cherry (SFmCherry) to the Ca^{2+} sensor GCaMP6f. We obtained two strains expressing the dual sensor SFmCherry-GCaMP6f, one where the two fluorophores are separated by a short (12 amino acids) linker (SL) and another with a long (232 amino acids) and rigid linker (LL), S1. Such constructions could in principle allow to estimate the diffusion coefficient of the dual sensor regardless of whether it is bound to Ca^{2+} or not (by analyzing the emission from the SFmCherry part) and therefore, to infer the properties of the Ca^{2+} transport from the analysis of the emission from the GCaMP6f part (as explained in Villarruel and Dawson (1)). This could be possible provided that there is no "cross-talk" between the two fluorophores of the fusion protein, namely that the emission from the GCaMP6f part of the sensor does not excite the emission from the SFmCherry one. As the GCaMP6f emission spectrum, $\sim 490 - 550\ nm$, partially overlaps the SFmCherry excitation one, $\sim 510 - 610\ nm$, if this two protein are close enough this "cross-talk" is possible. In order to check whether the emission from the GCaMP6f part of the SFmCherry-GCaMP6f sensor could be exciting the SFmCherry part we estimated the *Fluorescence Resonance Energy Transfer* (FRET) efficiency between the fluorophores.

Three different yeast strains were used: cells expressing only GCaMP6f or SFmCherry and cells expressing the fusion protein SFmCherry-GCaMP6f. The measurements with cells expressing GCaMP6f only were done illuminating the sample with the 488 *nm* line of an Argon laser with excitation power 6-10 μW. The measurements with cells expressing SFmCherry only or the fusion protein, SFmCherry-GCaMP6f, were done illuminating the sample only with the 543 *nm* line of a Helium-Neon laser with excitation power 2 μW and, immediately afterwards, only with the 488 *nm* line of an Argon laser. The fluorescence was collected from a 512x512 pixel frame located at approximately 2 μm from the coverslip at a 100 kHz and 50 kHz acquisition rate in the $500 - 530\ nm$ and $580 - 630\ nm$ ranges (green and red channels, respectively). Ten images were acquired for each strain, in each image ten cells were selected and in each cell the mean fluorescence from a $\sim 2\ \mu m^2$ region was calculated.

The FRET efficiency (FE) was then determined as:

$$FE = \frac{RC^{488} - \bar{a} GC^{488} - \bar{b} RC^{543}}{GC^{488}}, \tag{S9}$$

where $\bar{a}$ is the mean value of the ratio between the fluorescence collected in the red channel (RC) and in the green one (GC), $a = RC^{488}_{GCaMP6f}/GC^{488}_{GCaMP6f}$ for cells expressing GCaMP6f only and excitation wavelength of 488 *nm*. $\bar{b}$ is the mean value of the ratio $b = RC^{488}_{SFmCherry}/RC^{543}_{SFmCherry}$, between the fluorescence collected in the red channel when the sample was illuminated with the 488 *nm* line and the fluorescence collected in the same channel when it was illuminated with the 543 *nm* line for cells expressing SFmCherry only. RC^{488} and RC^{543} are the fluorescence intensities detected in the red channel when cells expressing the fusion protein were illuminated with the 488 *nm* and 543 *nm* lines, respectively, and GC^{488} the fluorescence detected in the green channel when the same cells were illuminated with the 488 *nm* line. FE quantifies the fraction of the emission of the SFmCherry part of the SFmCherry-GCaMP6f fusion protein that is due to the excitation by the emission of the GCaMP6f part of the protein.

The average values, $\bar{a}$=0.22 and $\bar{b}$=0.33, and standard deviations, σ_a=0.045 and σ_b=0.018, were obtained. Given that we used the mean values, $\bar{a}$ and $\bar{b}$, a few of the FE values obtained were negative. Negative values were not included to estimate the mean of FE but are included in the histograms that we present in the work. We show in Figure S1 histograms of the FE values obtained for the strain expressing SFmCherry-SL-GCaMP6f (C) and SFmCherry-LL-GCaMP6f (D) from which we derived the estimates of the means, FE_{SL}= 0.17 ± 0.01 and FE_{LL}= 0.09 ± 0.01, respectively. The LL version was subsequently used in the FCS experiments in yeast due to its negligible FRET effects.

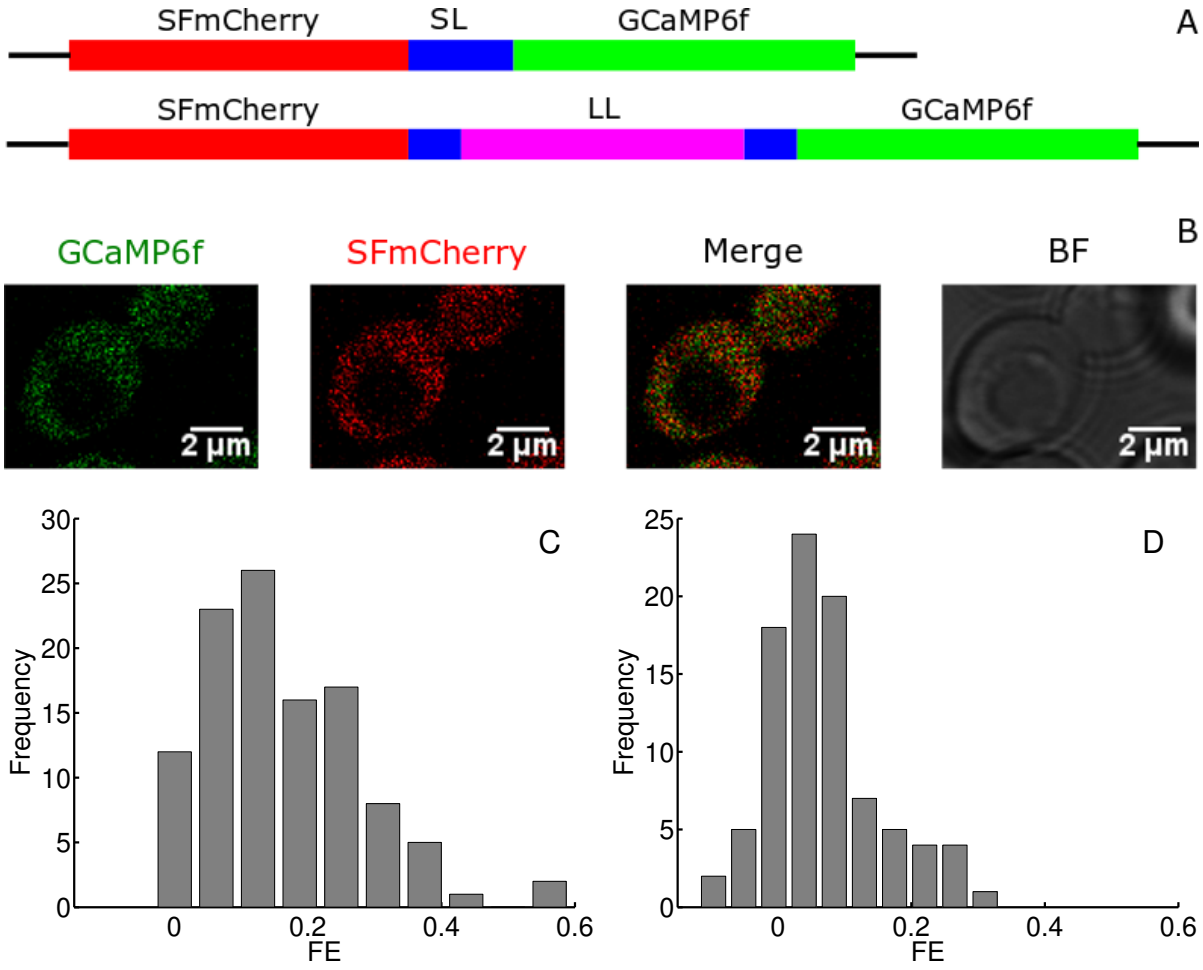

Figure S1: (A) SFmCherry and GCaMP6f fusion protein, with the short linker (top) and the long ER/K based linker (bottom). (B) *S. cerevisiae* cells expressing SFmCherry-LL-GCaMP6f fusion protein. Panels show GCaMP6f and mCherry fluorescence and their merged images. Brightfield (BF) images of the cells are shown in the far right panel. Barr 2 μm. (C) and (D) Distribution frequency histograms of the FRET efficiency values obtained for the strain expressing the fusion protein SFmCherry-GCaMP6f with the short (C) and the long (D) linker.

ESTIMATION OF THE FLUO8 FREE DIFFUSION COEFFICIENT IN AQUEOUS SOLUTIONS

In order to identify which diffusive timescale could be associated to the free diffusion of the Fluo8 dye in the FCS experiments performed in oocytes we characterized the diffusion coefficient of Fluo8 with Ca^{2+} in aqueous solutions. To this end we performed FCS experiments in solutions containing 286 nM of Fluo8 and different concentrations of Ca^{2+}, ranging from 500 nM to 10 μM. The measurements were done depositing on a coverslip a 70 μl drop of the chosen solution. The fluorescence records were obtained illuminating the sample with the 488 nm line of an Argon laser, with an excitation power of 4 μW, and collecting the emitted light from a single point located at approximately 15 μm from the coverslip in the 500–600 nm range at a 50 kHz acquisition rate during ~180 s (equivalently, 8388096 data points). Using Eq. (4) to fit the ACF of the

fluorescence fluctuations we obtained two diffusion coefficients, D_1 and D_2, for each Ca^{2+} concentration probed (between 5 and 10 experiments for each Ca^{2+} concentration are reported). We show the results of the fits (with symbols) in Figure S2. We compared these results with the three diffusion coefficients that appear in the correlation times of a system with a single wavelength (SW) dye and Ca^{2+} (3). These theoretical diffusion coefficients, computed with the concentrations derived from the ones used to prepare the aqueous solutions in the experiments, the dissociation constant of the vendor for this situation and the free coefficients in solution listed in Table 1, are plotted with curves in Figure S2. Two of these diffusion coefficients (dashed and dotted lines in Figure S2) are effective ones, *i.e.*, are concentration-dependent, and the third one (solid line) corresponds to the free diffusion coefficient of the dye. Performing the experiments for different Ca^{2+} concentrations, the free diffusion coefficients of the dye, D_F, and of Ca^{2+}, D_{Ca}, can be derived from the effective ones as done in Sigaut et al. (3). In the present case the best fit was obtained using Eq. (4) from which we derived two coefficients, D_1 and D_2, shown with symbols in Figure S2. Thus, there was some indetermination as to what the two coefficients derived from the fits corresponded to. As shown in Figure S2, one of them, D_2, was relatively high and close to the free Ca^{2+} diffusion coefficient for most of the concentrations probed. According to the theory, this relatively large coefficient is actually an effective one, D_{ef1}, that approaches D_{Ca} with increasing $[Ca^{2+}]_{tot}$. D_1, on the other hand, remains close to D_F and to D_{ef2} two coefficients that are very similar to one another for almost all the range of $[Ca^{2+}]$ analyzed. If we identify D_1 with D_F=D_{Fluo8} we can derive an experimental estimate of D_{Fluo8} computing the average of D_1 over the values obtained for all the Ca^{2+} concentrations probed. Proceeding in this way we obtained D_{Fluo8}=(125 ± 9) $\mu m^2/s$. If we associate D_1 to D_{ef2}, the estimate of D_{Fluo8} can be obtained using Eq. (S8) with the dissociation constant provided by the vendor, kD_{Fluo8}=432 nM, the expected free diffusion coefficient of Ca^{2+}, D_{Ca}=760 $\mu m^2/s$ and the concentrations $[Fluo8]_{tot}$ and $[Fluo8]_{eq}$ of the construction. Proceeding in this way we obtained D_{Fluo8}=(100 ± 19) $\mu m^2/s$. To derive an estimate of the Ca^{2+} free diffusion coefficient, D_{Ca}, from the experiments we use Eq. (S5), the dissociation constant, kD_{Fluo8}=432 nM, the concentrations of the construction and the free diffusion coefficient of Fluo8 previously estimated. Using D_{Fluo8}=(125 ± 9) $\mu m^2/s$ or D_{Fluo8}=(100 ± 19) $\mu m^2/s$ we obtained D_{Ca}=(794 ± 24) $\mu m^2/s$ and D_{Ca}=(795 ± 24) $\mu m^2/s$, respectively. We decided to use D_{Fluo8}=100 $\mu m^2/s$ for all the theoretical computations (*e.g.*, for the theoretical curves of Figure S2) as listed in Table 1. All the estimates agree with those obtained from FCS experiments performed in aqueous solutions with Ca^{2+}, Fluo8 and the Ca^{2+} chelator, EGTA (1) and the free diffusion coefficient of Ca^{2+} agrees with previous estimates (2–4).

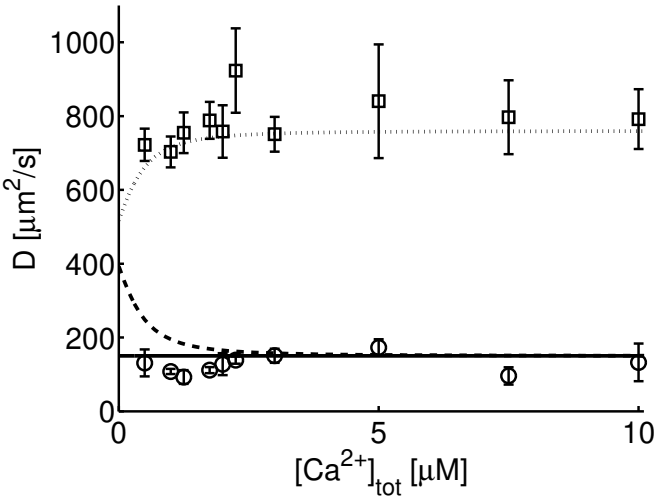

Figure S2: Theoretical diffusion coefficients for a system containing Fluo8 and Ca^{2+} (with lines) and two diffusion coefficients estimated from FCS experiments performed in aqueous solutions of Fluo8 and Ca^{2+} (symbols and error bars: mean and SEM of the mean). The theoretical coefficients are the free coefficient of the dye, D_F (solid line), and two effective coefficients, D_{ef1} (dotted line) and D_{ef2} (dashed line). The two estimated coefficients, D_1 (circles) and D_2 (squares), were obtained by fitting the experimental ACF with Eq. (4).

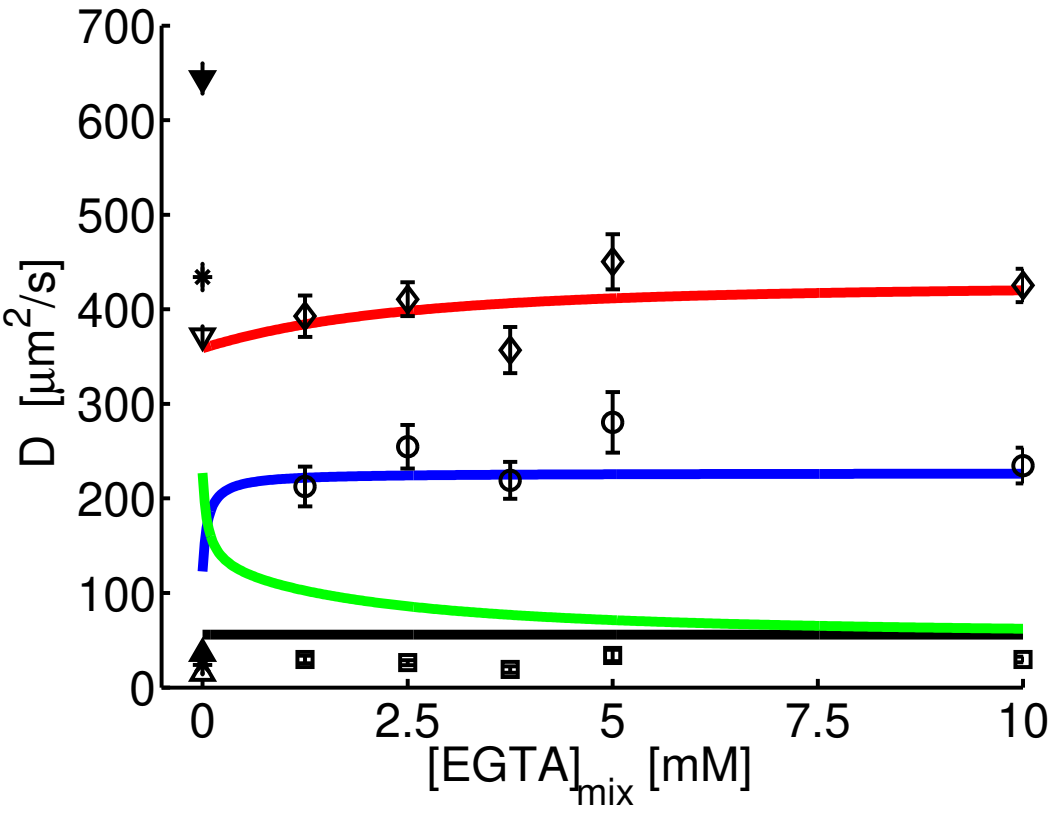

Figure S3: Diffusion coefficients derived from experiments performed in oocytes microinjected with a mix with [Fluo8]=100μM and zero or different concentrations of EGTA. The symbols in the figure represent mean values and the error bars the corresponding SEM. As in Figure 5 in the main text, we also plot, with solid lines, the theoretical results obtained for a reaction-diffusion system with Ca^{2+}, EGTA and Fluo8 using the parameters of Table 1 and [Fluo8]=3.7 μM. The free diffusion coefficients in this Table correspond to values in aqueous solutions and can be larger, by a certain factor, with respect to their corresponding values in the cytosol. The theoretical results (D_{Fluo8}, D_{ef1}, D_{ef2} and D_{ef3}, in black, blue, red and green, respectively) were then rescaled by the factor 0.56 so as to make the largest (mean) coefficient obtained experimentally at $[EGTA]_{mix} = 10mM$, $425\mu m^2/s$, equal to the largest theoretical coefficient at the same concentration. We did this under the assumption that, at $[EGTA]_{mix} = 10mM$, the largest experimental coefficient is approximately equal to the Ca^{2+} free diffusion coefficient, D_{Ca}, in this setting and that the factor, 0.56, reflects differences in viscosity between the cytosol (where the value $D_{Ca} \approx 425\mu m^2/s$ was obtained) and water (where $D_{Ca} \approx 760\mu m^2/s$). As discussed at large in the paper, our results point to the existence of regions of different viscosities in the cytosol, albeit, with a prevalence of those that are approximately twice as viscous as water which would give a rescaling factor ~ 0.56. The ACFs derived from the experiments performed with EGTA were fitted with Eq. (5) from which three diffusion coefficients were obtained. Those with no EGTA (illustrated in Figure 4 of the paper) were fitted with Eq. (4). Thus, only two diffusion coefficients, $D_1 < D_2$, were derived in this case. The values obtained for each of these two coefficients could be grouped in two subpopulations (see paper for details). In this figure we show, for both D_1 and D_2 ([EGTA]=0), the mean over each of these subpopulations separately using up-pointed triangles for D_{1a} and D_{1b} and down-pointed triangles for D_{2a} and D_{2b}, with open symbols for the subpopulation of larger weight (D_{1a} and D_{2a}). We also show the mean over the whole population of each of the two coefficients with asteriks. We observe that, in the case of D_2, the mean over the population of largest weight (D_{2a}=372 $\mu m^2/s$) falls very close to the theoretical curve that approaches the value, D_{Ca} = 425 $\mu m^2/s$, for increasing [EGTA]. As discussed in the paper this is consistent with the assumption that the large variability of the values, D_2, derived from the experiments with [EGTA]=0 can be attributed to a similar variability in vicosity but whose most likely value (the mean over $\sim$ 77% of the cases) is 1.8 times that of water.

REFERENCES

1. Villarruel, C., and S. P. Dawson, 2020. Quantification of fluctuations from fluorescence correlation spectroscopy experiments in reaction-diffusion systems. *Physical Review E* 102:052407.

2. Sigaut, L., C. Villarruel, and S. P. Dawson, 2017. FCS experiments to quantify Ca2+ diffusion and its interaction with buffers. *The Journal of Chemical Physics* 146:104203. https://doi.org/10.1063/1.4977586.

3. Sigaut, L., C. Villarruel, M. L. Ponce, and S. Ponce Dawson, 2017. Fluorescence correlation spectroscopy experiments to quantify free diffusion coefficients in reaction-diffusion systems: The case of Ca^{2+} and its dyes. *Phys. Rev. E* 95:062408. https://link.aps.org/doi/10.1103/PhysRevE.95.062408.

4. Qin, D., A. Yoshida, and A. Noma, 1991. Limitations due to unstirred layers in measuring channel response of excised membrane patch using rapid solution exchange methods. *Japanese Journal of Physiology* 41:333–339.